Nuclear Engineering and Design 442 (2025) 114268

Contents lists available at ScienceDirect

Nuclear Engineering and Design

journal homepage: www.elsevier.com/locate/nucengdes

Benchmarking exercise on the radiological consequence calculation due to a potential severe accident in Zaporizhzhia Nuclear Power Plant

J.C. de la Rosa Blul [a,*], A. Guglielmelli [b], O. Parera Villacampa [a], S. Arndt [c], S. Band [c], S. Beck [c], H. Boxman [d], G. Fritsch [e], J. Groell [f], T. Hamburger [g], P. Hofer [e], O. Isnard [f], A. Kloosterman [h], G.O. Nicaise [f], A. Pašiškevičius [i], T. Peltonen [j], C. Potiriadis [k], O. Romanenko [l], N. Salpadimos [k], A. Ševčik [m], M. Tempra [n]

[a] European Commission, Joint Research Centre, Petten, the Netherlands
[b] European Commission, Joint Research Centre, Ispra, Italy
[c] Gesellschaft für Anlagen und Reaktorsicherheit (GRS), Germany
[d] Authority for Nuclear Safety and Radiation Protection (ANVS), the Netherlands
[e] Division Radioprotection, Federal Ministry for Climate Action, Environment, Energy, Mobility, Innovation and Technology, Austria
[f] Authority for Nuclear Safety and Radiation Protection (ASNR), France
[g] Bundesamt für Strahlenschutz (BfS), Germany
[h] National Institute for Public Health and the Environment (RIVM), the Netherlands
[i] State Nuclear Power Safety Inspectorate (VATESI), Lithuania
[j] Radiation and Nuclear Safety Authority (STUK), Finland
[k] Greek Atomic Energy Commission (EEAE), Greece
[l] SS "Rivne NPP" JSC NNEGC "Energoatom", Ukraine
[m] Radiation Protection Centre (RSC), Lithuania
[n] National Inspectorate for Nuclear Safety and Radiation Protection (ISIN), Italy

ARTICLE INFO

Keywords:
Severe accident
Atmospheric dispersion tools
Radiological consequences
Emergency preparedness and response
Benchmarking

ABSTRACT

This paper presents the analysis and results of an inter-comparison activity on the radiological consequences of a postulated severe nuclear accident at the Zaporizhzhia Nuclear Power Plant. The activity was conducted within the framework of the Western European Nuclear Regulators Association (WENRA) Experts Group, the Heads of the European Radiological Protection Competent Authorities (HERCA) Task Force in support of Ukraine, and the European Community Urgent Radiological Information Exchange (ECURIE) Competent Authorities.

To assess the impact of the source term on the radiological consequences, two different approaches have been proposed: in the first approach a fixed source term calculated from an unmitigated Station Blackout (SBO) at ZNPP affecting the entire reactor fleet of six units and spent fuel pools in shutdown conditions was distributed among the participants, and the second approach was considering the same scenario, however at full-power conditions with each organization having the freedom to compute its own source term.

Twelve European organisations participated in the first exercise –called WG-UA-1– whereas five in the second –called WG-UA-2. Three output variables were taken as figures of merit: the cumulative effective dose, thyroid equivalent dose, and total ground deposition of Cs-137 and I-131 for the first and second exercise, respectively.

Several national organizations in Europe provide technical support for Emergency Preparedness and Response (EPR) activities, often using different tools and models to assess radiological impact. The varying technical and scientific features of these tools can significantly affect the final results consistency, influencing confidence in their reliability for EPR decision-making.

An overall comparison of WG-UA1 against WG-UA2 confirms the fundamental role played by the source term on the radiological consequence figures of merit. The comparison highlighted significant differences in the maximum geographical path trajectory –made up of the geographical points at each distance from the source point featuring the highest output value– after the first days. However, a much higher level of agreement in terms of the maximum values applies for WG-UA-1.

* Corresponding author.
E-mail address: Juan-Carlos.DE-LA-ROSA-BLUL@ec.europa.eu (J.C. de la Rosa Blul).

https://doi.org/10.1016/j.nucengdes.2025.114268
Received 7 May 2025; Received in revised form 18 June 2025; Accepted 23 June 2025
Available online 7 July 2025
0029-5493/© 2025 The Authors. Published by Elsevier B.V. This is an open access article under the CC BY license (http://creativecommons.org/licenses/by/4.0/).

Several recommendations have been drawn from this study, including the development of best practices in using dose projection tools, the use of maximum path values as reliable indicators for informing protective countermeasures, and further research into the potential benefits of using average values at sector levels to orient protective countermeasures rather than pointwise geographical values.

1. Introduction

The Zaporizhzhia Nuclear Power Plant (ZNPP) in Ukraine is one of the largest nuclear installations in Europe, and a severe nuclear accident there could have transboundary effects, impacting not only Ukrainian territory, but also neighbouring countries. This necessitates international cooperation and information exchange on assessing the risks and the potential radiological consequences.

The paper presents the results of an inter-comparison activity –called benchmarking interchangeably– initiated by the WENRA experts' group (www.wenra.eu/rhwg, 2025) and the HERCA Task Force (www.herca.org/activity/emergency-preparedness-and-response, 2025) in support of Ukraine. This initiative was also discussed by the European Community Urgent Radiological Information Exchange (ECURIE) competent authorities (European_Community, 2025).

As depicted in Fig. 1, two approaches were proposed to analyse the radiological consequences of a potential severe nuclear accident at the Zaporizhzhia Nuclear Power Plant (ZNPP).

The first exercise, WG-UA-1, involved a fixed source term computed and distributed by the Joint Research Centre (JRC) to all participants (see Table 1). The selected accident scenario was an unmitigated Station BlackOut (SBO) at the Zaporizhzhia Nuclear Power Plant (ZNPP), affecting the entire reactor fleet of six units and the spent fuel pools. Four reactors featured filtered containment venting, while the other two were unfiltered. The reactors were assumed to be in shutdown conditions. Due to the slow accident kinetics of the selected scenario, the radiological consequences were analysed over a period of 30 days from the initiating event and around 21 days from the start of the release.

The second exercise, WG-UA-2, allowed participants the freedom to compute their own source term. A total of five organizations participated in this exercise (i.e., France, Germany, Greece, The Netherlands and the European Commission). The selected accident scenario was an unmitigated SBO at the ZNPP, impacting a single reactor with unfiltered containment venting. The reactor was assumed to be operating at full power at the time of the SBO event. The results were provided for the 7 days following the initiating event.

Three radiological-consequence indicators were taken as Figures of Merit (FOM) for both exercises WG-UA-1 and WG-UA-2, i.e. cumulative effective dose, thyroid equivalent dose, and total ground deposition of Cs-137 and I-131.

2. Scope

Benchmarking activities comprise the analysis of results provided by different participants using different information sources, different tools and applying different assumptions. This activity requires significant resource mobilization and substantial computational efforts to hierarchically identify the underlying driving factors that explain any discrepancies between the results, see, e.g. BARCO (Benchmarking on Assessment of Radiological Consequences) (Balashevska et al., 2024), IAEA CRP on Effective Use of Dose Projection Tools in the Preparedness and Response to Nuclear and Radiological Emergencies (IAEA Coordinate Research Project, 2025), and OECD/NEA Expert Group on Comparison and Understanding of Dose Prognosis (Nuclear Energy Agency, 2025).

Unlike standard benchmarking activities that typically focus on identifying key factors leading to discrepancies among results, the exercise presented in this work aims to enhance mutual collaboration among WENRA (www.wenra.eu, 2025), HERCA (www.herca.org, 2025), and ECURIE (European_Community, 2025) Competent Authorities. The keystone priority is to share radiological consequence information in the event of a nuclear accident and to increase mutual knowledge of current discrepancies in dose projection methods and tools. By raising awareness of the actual degree of divergence in the projected calculations, decision-makers will be better positioned to understand the reliability of these tools when implementing protective countermeasures in response to a nuclear emergency.

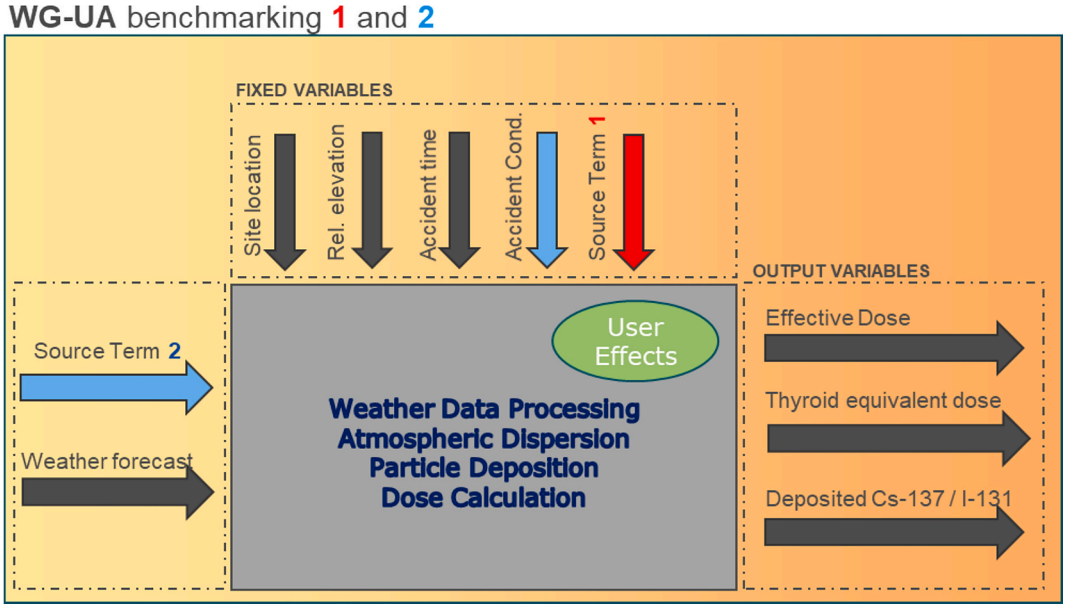

Fig. 1. Schematics of benchmarking exercise 1 and 2.

Table 1
Codes, Models, Weather Data, and Geographical Resolution used by Participants[1].

Country	RC Code	ADM Model and Type	Weather data source	Weather data resolution	Grid Resolution (km)
Austria	JRODOS	DIPCOT / Lagrangian	ECMWF	0.2°	0.5/1.0/2.0/4.0/8.0
Germany	JRODOS	LASAT / Lagrangian	DWD	0.0625°	0.5/1.0/2.0/4.0/8.0
Finland	JRODOS	RIMPUFF / Gaussian	NOAA	0.5°	0.5 / 1.0
France	C3X (v4.5)	pX / Gaussian	ARPEGE (EURAT01)	0.1°	1.0 x 1.0
Greece	JRODOS	RIMPUFF / Gaussian	NOAA	0.25°	0.5 x 0.5
Hungary	JRODOS	RIMPUFF / Gaussian	NOAA	0.5°	1.0 x 1.0
Italy	ARIES	LAPMOD / Lagrangian	ECMWF	0.25°	2.5 x 2.5
Ireland	ARGOS	RIMPUFF / Gaussian	NOAA	0.25°	5.0 x 5.0
Lithuania	JRODOS	DIPCOT / Lagrangian Puff	NOAA	0.5°	1.0 x 1.0
The Netherlands	NPK-PUFF	NPK-PUFF / Gaussian	ECMWF	0.1°	1.0 x 1.0
Slovakia	DIPCOT	Lagrangian	NOAA	0.5°	1.0 x 1.0
Ukraine	LASAT	Lagrangian	NOAA	0.5°	0.25/0.5/1.0/2.0/4.0
EU	RIMPUFF / LASAT	Gaussian / Lagrangian	NOAA	0.5°	0.5/1.0/2.0/4.0/8.0

[1]One of the participants in the list provided the results in a non-compatible format with the exercise, so the final number of participants decreased by one.

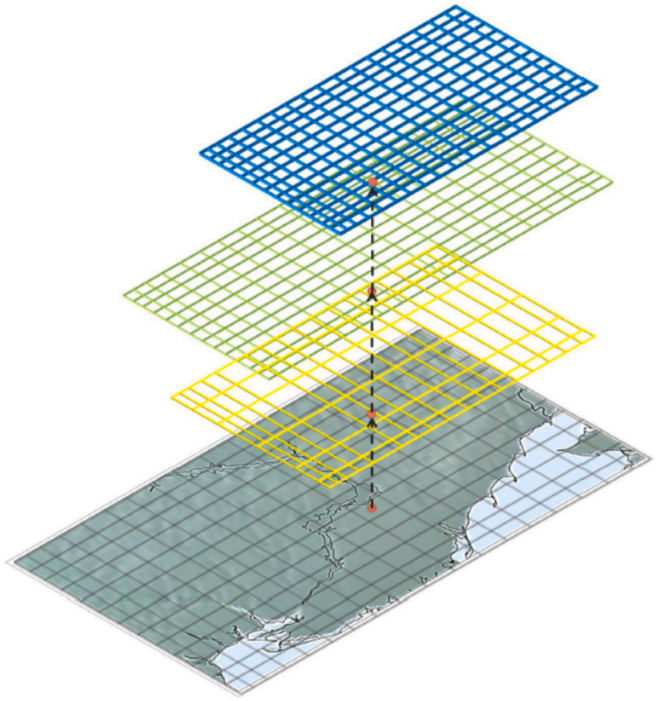

Fig. 2. RADCOM cell-to-point conversion capability.

3. Methods: RADCOM statistical analysis benchmarking tool

The current benchmarking activity generated a large radiological dataset for each of the three Figures of Merit (FOMs). The JRC's in-house tool, RADCOM (RADiological Consequence COMparison), was used to process the input data, perform statistical analyses, and develop plot files and maps.

RADCOM is a statistical application written in Python 3.9, specifically designed for comparing radiological consequences and analysing large quantities of time-dependent data provided at the geographical cell level. RADCOM can perform a series of operations to manage and analyse the input data, such as initialization operations, cell-to-point conversion, data merging, and comparison of output values at distinct locations, points, and times (see Fig. 2 and Fig. 3). Additionally, RADCOM works at geographical sector level by computing and comparing the arithmetic mean of the values calculated by each participant within each sector.

For the current benchmarking exercise, the computational grid was further divided into different polar sectors, azimuthally at every 30 degrees and radially at 3, 5, 10, 30, 50, and 100 km (see Fig. 4 and Fig. 5). This additional assessment aimed to compare the degree of agreement at point level with that obtained at area level. This comparison enabled verification of whether the deviation observed at point level is consistent or biased. Specifically, whether the magnitude of the deviation in the results computed by different participants at specific geographical locations could be extrapolated to a whole region.

RADCOM performs statistical analysis to calculate and compare several variables at each geographic point included in the whole computational grid, such as the average and standard deviation at selected points or sector levels at different time instants. It also computes the number of favourable cases between the average and two times the standard deviation, as well as the Coefficient of Variation of the complete set of values for a specific time instant, which is the ratio between the standard deviation and arithmetic mean. The Coefficient of Variation provides an estimate of the relative dispersion of the elements within a sample. Given its dimensionless nature, it can be used to compare the variability of data across variables with different units.

Fig. 3. Selected locations along straight lines at fixed distances and selected locations.

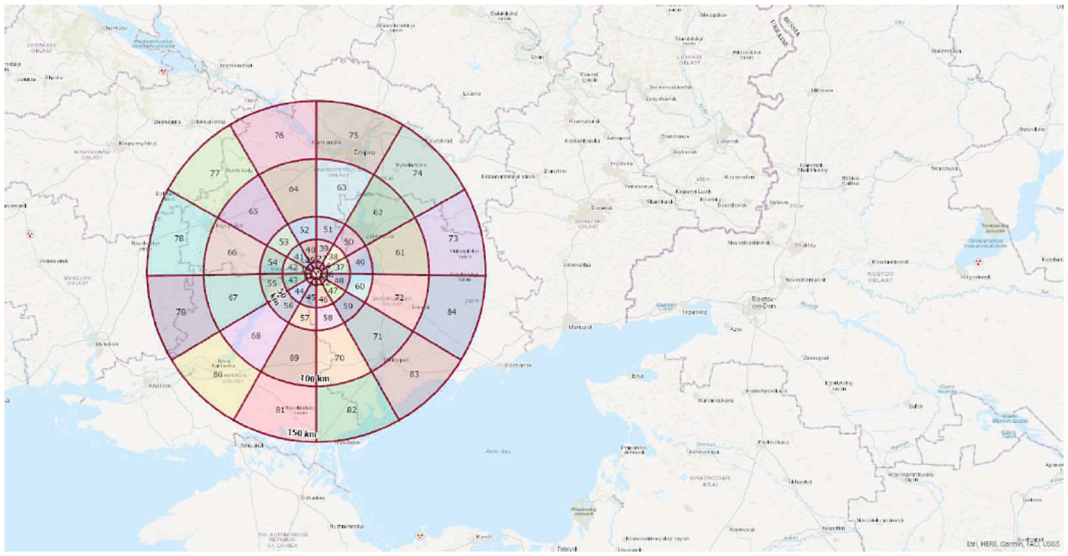

Fig. 4. RADCOM capability to evaluate the results at grid sector level.

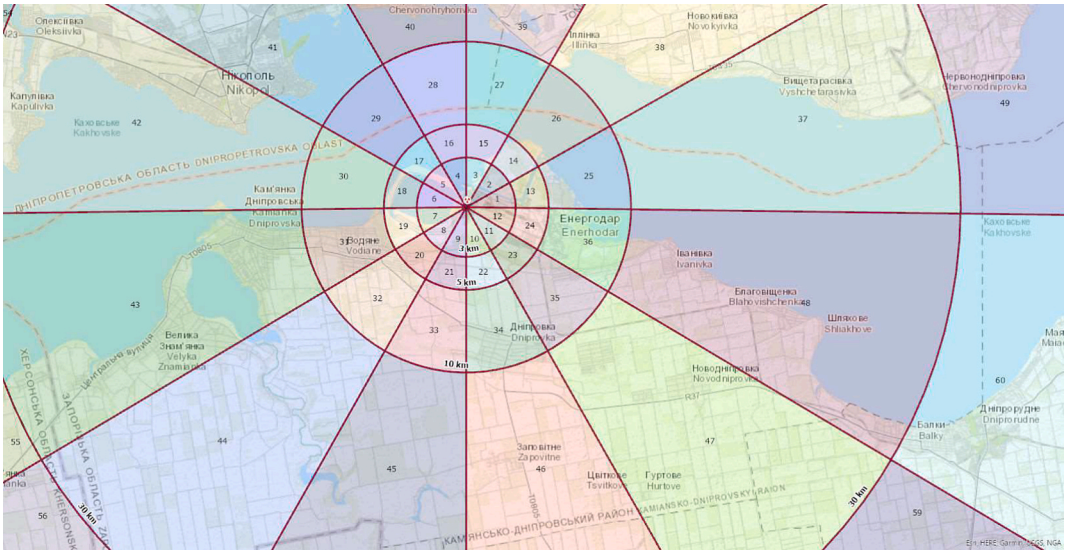

Fig. 5. RADCOM capability to evaluate the results at grid sector level (larger zoom).

Extensive quality checks have been performed for all the FOMs and main computational tasks carried out by RADCOM.

RADCOM evaluates the results along the maximum path as the ensemble of geographical points featuring the maximum output value at each distance from the source point. It also looks at the maximum path in terms of the maximum values computed by each participant across the entire computational grid and at the sector level.

RADCOM also performs country-to-country comparison both for the whole computational grid and at sector level:

- Vis-à-vis for a single output value at different time instants, taking the entire number of possible 2-combinations, which is equal to the binomial coefficient C (n, k) with k = 2 and n equal to the number of participants (n = 12 for WG-UA-1 leading to 66 combinations; n = 5 for WG-UA-2 leading to 10 combinations). The percentage of values within one and two orders of magnitude is also evaluated. Trend analysis of the absolute and relative degree of convergence of the vis-à-vis comparison with time and magnitude of output values is also performed.
- Vis-à-vis comparison for a single output value of the whole dataset, taking the entire number of possible 2-combinations.

4. Atmospheric dispersion analysis: Input data and tools

This section describes the data (i.e., the source term, the meteorological data, the atmospheric dispersion models, etc.) and the tools used by each participant to perform the radiological atmospheric dispersion analysis of the severe accident scenario proposed by JRC.

4.1. WG-UA-1/2: Codes, models, weather data

Table 1 depicts the various software tools, atmospheric dispersion models, weather data and computational grid resolution used by each participant in the WG-UA-1 and WG-UA-2 benchmarking exercises.

The tools used for the atmospheric dispersion analysis are those commonly adopted for research activities in the field of routine atmospheric discharge from nuclear facilities (Selivanova et al., 2023), radiological impact of severe accident scenario (Murat et al., 2024; Mercan et al., 2022) and location of the early warning stations

Table 2
WG-UA-1 source term.

Source term Magnitude		
Noble Gas (Bq)	**Caesium (Bq)**	**Iodine (Bq)**
6.21E + 18 Xe-133: 5.16E + 18	3.27E + 13 Cs-137: 9.9E + 12	2.58E + 15 I-131: 7.86E + 14 Molecular (I_2): 1.5E + 15 Organic (ICH_3): 4.5E + 13 Aerosol: 1.1E + 15

(Dąbrowski and Kikoła, 2023). These codes are widely used for radiological assessment around nuclear power plants and research reactors (Pirouzmand et al., 2015; Choi and Lim, 2018; Pirouzmand et al., 2018). Furthermore, these tools are often adopted by many users, who improve their own abilities to use the codes by participating in several user group exercises (Orr et al., 2023). The reliability of the provided outcomes is assessed through code-to-code comparison (Orr et al., 2021) and validation activities (Dong et al., 2021; Quélo et al., 2007).

4.2. WG-UA-1: Source term

In WG-UA-1, the source term was provided by the Joint Research Centre (JRC) to all the participants. The selected accident scenario involved an unmitigated Station Blackout (SBO) in ZNPP, affecting the entire reactor fleet of six VVER-1000/320 units and spent fuel pools. Four reactors featured filtered containment venting, while the two others were unfiltered. All the reactors were assumed to be in shutdown conditions. Table 2 displays the source term value for noble gas, caesium

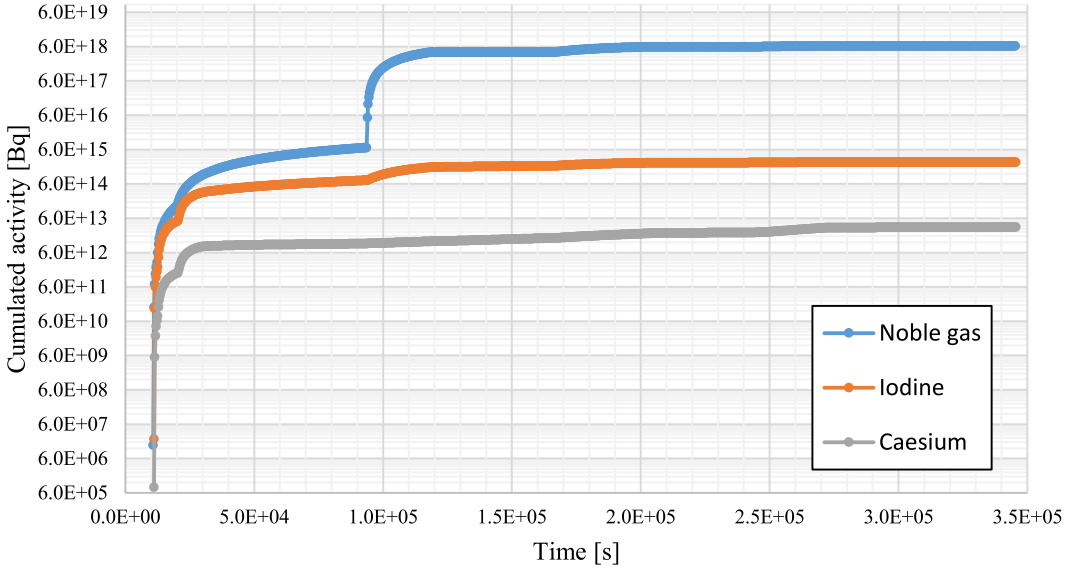

Fig. 6. WG-UA-1 source term – cumulated activity for some radionuclides class.

Table 3
WG-UA-2 Accident Evolution Key Information.

Country	Severe Accident information								
	Used code	Events time					Model information		
		SG water depletion	Beginning of core melt	First and second venting system opening	RPV / primary failure	primary induced rupture	Allowable leak rate	Containment free volume	Reactor cavity water inventory at RPV failure
France	PERSAN 4	1.5 h	5.0 hrs	First FCVS: 5 bar (36 h) Second FCVS: 5 bar (48 h)	8 h	Hot leg creep rupture	0.15 %vol/d direct to atmosphere + 0.15 %vol/d to Main Power Building	60.000 m^3	Dry
Germany	AC²-2021.1	1.9 h	7.0 h	First FCVS: 4.9 bar (18.9 h) Second FCVS: 30.5 h	3.8 h (SAM) 9.2 h (RPV wall failure)	SAM: operator action – open 3 PRSV when core exit temperature > 450 °C	0.3 % vol/day (at design pressure) to environment	61.163 m3	804 kg (plus 228200 kg at 13.2 m containment floor elevation)
Greece	ORIGEN-ARP	NA	8.0 hrs	NA	NA	NA	NA	NA	NA
Netherlands	Documentation from KCB	NA	2.4 hrs	32.4 h	NA	NA	0.10 % vol/day	57.102 m3	NA
JRC	MAAP5.03-VVER	1.5 h	2.7 h	First: 14.8 h Second: 24.3 h	5 h	Hot leg creep rupture	0.3 % vol/day	66.700 m3	900 kg

Table 4
WG-UA-2 source term.

Source term Magnitude			
Country	**Noble Gas (Bq)**	**Caesium (Bq)**	**Iodine (Bq)**
France	1.50E + 18 Xe-133: 1.30E + 18	1.40E + 14 Cs-137: 5.1E + 13	1.50E + 17 I-131: 9.02E + 16 Molecular (I_2): 8.5E + 16 Organic (ICH_3): 6.1E + 16 Aerosol: 2.1E + 15
Germany	Total: 4.50E + 18 Xe-133: 3.60E + 18	Total: 3.76E + 15 Cs-137: 1.31E + 15	Total: 1.09E + 17 I-131: 1.54E + 16 Molecular (I_2): 1.4E + 16 Organic (ICH_3): 2.29E + 16 Aerosol: 7.2E + 16
Greece	Total: 1.50E + 16 N/A	Total: 1.67E + 15 Cs-137: 6.21E + 14	Total: 1.69E + 16 I-131: N/A All molecular
Netherlands	Total: 1.01E + 18 Xe-133: 5.71E + 18	Total: 8.91E + 14 Cs-137: 3.04E + 14	Total: 1.74E + 16 I-131: 9.44E + 15 N/A
JRC	Total: 6.67E + 18 Xe-133: 5.28E + 18	Total: 2.05E + 16 Cs-137: 6.29E + 15	Total: 6.09E + 17 I-131: 1.98E + 17 Molecular (I_2): 5.17E + 17 Organic (ICH_3): 1.83E + 16 Aerosol: 7.31E + 16

and iodine and some nuclide-specific values provided to each participant to the UA-1 exercise.

Fig. 6 displays the WG-UA-1 source term in terms of cumulative activity released, categorized by noble gases (Kr-85, Kr-85 m, Kr-87, Kr-88, Xe-131 m, Xe-133, Xe-133 m, Xe 135 m, Xe-138), iodine isotopes (I-131, I-132, I-133, I-134, I-135), and caesium isotopes (Cs-134, Cs-136, Cs-137).

The analysis was performed with the MAAP 5.03 accident system code. Several sources of information were used for the reactor modelling. Among the plant-specific information, the following was accurately modelled: geometry and inventories for the primary and secondary systems, pressure and temperature for the primary and secondary systems, containment volume, design (modelled with 10 nodes) and failure pressure, allowable leakage rate, containment concrete chemical composition (basaltic with 14.5 % water) and safeguards (high pressure injection, low pressure injection, passive accumulators and containment sprays), system alignment, portable equipment and mitigating filtered containment system. The spent fuel pools were also carefully modelled with plant-specific information reflecting the ZNPP actual pools accurately, assuming the most penalizing configuration and outage. The initial fission product inventory included 65 radionuclides (de la Rosa Blul et al., 2022).

4.3. WG-UA-2: Source term

In the WG-UA-2 exercise, the participants calculated their own source terms based on a proposed severe accident scenario consisting of an unmitigated SBO in ZNPP impacting one single reactor at full power operating condition with unfiltered containment venting.

Table 3 shows the key results related to the severe accident evolution simulated by the participants including main aspects of the accident progression and source term calculation, the specific codes used by each participant and the key boundary conditions related to the containment and interface with the outside environment.

The tools used for the source term evaluation varied significantly in terms of source term forecasting capability, ranging from those limited to the fission products inventory (Jeong et al., 2016), to those considering only the main physicochemical phenomena affecting the source term (Guglielmelli et al., 2019), to the system codes able to cope with the full set of phenomena related to the thermal–hydraulic and severe accident part (Sato et al., 2024).

Table 4 shows the activity of noble gases, total caesium and iodine as part of the source term calculated by each participant for WG-UA-2.

In Table 4, the value reported in the iodine column refers to the amount of iodine emitted at the first containment venting. It is noted that some of the participants assumed a source term with an emission time of 72 h from the start of the release whereas others did not assume any mitigating measure along the entire simulation time of 96 h. Table 5 provides a graphical comparison between the source term values calculated for noble gases, caesium, and iodine by each participant in WG-UA-2.

Regarding the weather forecast data, most of the participants relied on atmospheric reanalysis data, which might have an influence compared to real conditions (Sørensen, 2020).

Table 5
WG-UA-2 source term computed from each participant for noble gases, caesium and iodine.

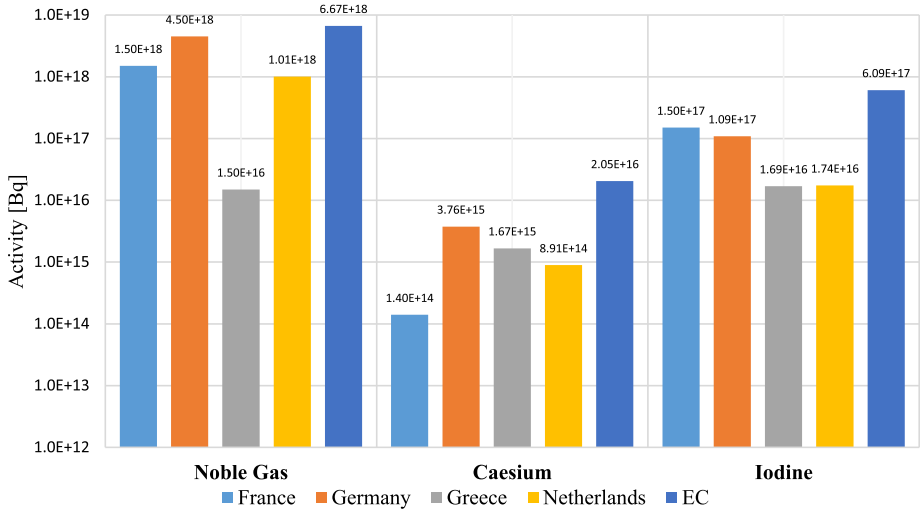

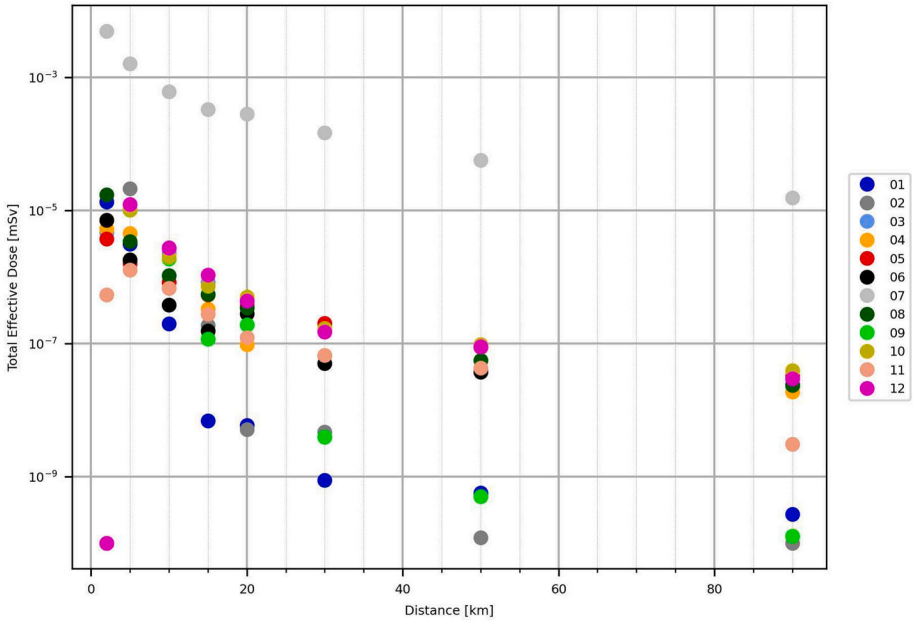

Fig. 7. WG-UA-1 – TEDE at 72 h at 0 degrees.

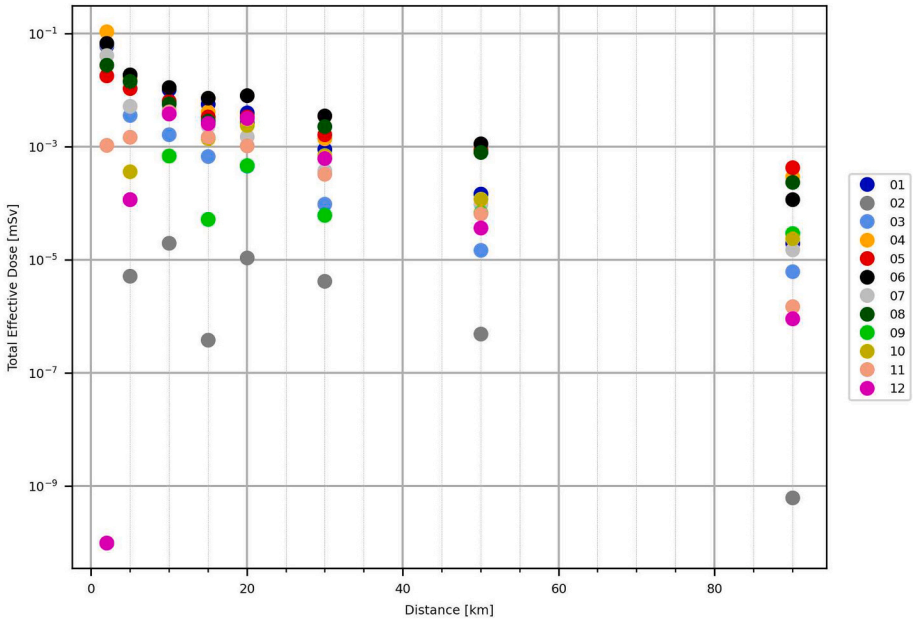

Fig. 8. WG-UA-1 – TEDE at 120 h at 30 degrees.

5. Analysis of the results

5.1. Comparison along straight lines

The results were compared at fixed distances along straight lines from the source point at specific time instants. This type of comparison is widely used in scientific activities to evaluate the radiological impact at various distances and directions from the emission point (Quélo et al., 2007; Jeong et al., 2016; Guglielmelli et al., 2019). The angles are taken every 30 degrees (e.g., 0, 30, 60, 90, 120, 150, 180, 210, 240, 270, 300, 330) and the distances are taken at 2, 5, 10, 15, 20, 30, 50 and 90 km from the source point. Times are taken at 24, 48, 72, 96, 120, 168, 192, 216, 240, 264, 288, 312, 336, 384, 408, 432, 456, 480, and 500 h from the start of the releases. The comparison will focus on the total effective dose equivalent (Figs. 7 and 8) and Cs-137 ground deposition (Figs. 9 and 10) for WG-UA-1, as well as the total effective dose equivalent (Figs. 11 and 12) and I-131 ground deposition (Figs. 13 and 14) for WG-UA-2. This approach is justified because Cs-137 ground deposition and I-131 ground deposition, along with TEDE and thyroid equivalent dose, exhibit similar comparison patterns. The analysis of the results revealed two main biases in the data:

1. The degree of divergence decreases with higher output values and longer elapsed times for WG-UA-1, whereas there is no clear trend for WG-UA-2 results.
2. For WG-UA-1, the degree of divergence typically ranges from less than one order of magnitude to two orders of magnitude, although in many locations it can exceed this range. For WG-UA-2, the degree of divergence can be very wide, spanning several orders of magnitude.

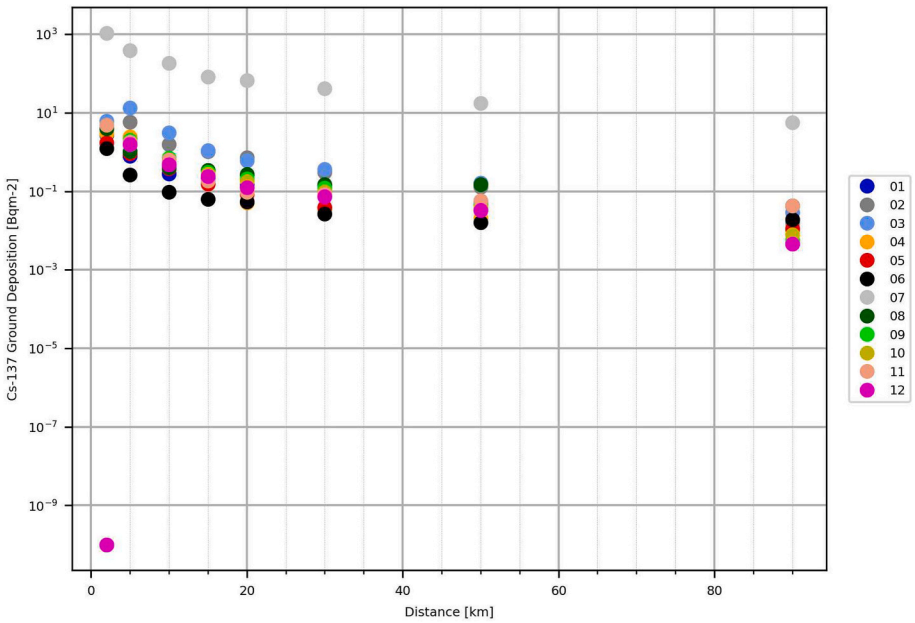

Fig. 9. WG-UA-1 – Cs-137 ground deposition at 72 h at 0 degrees.

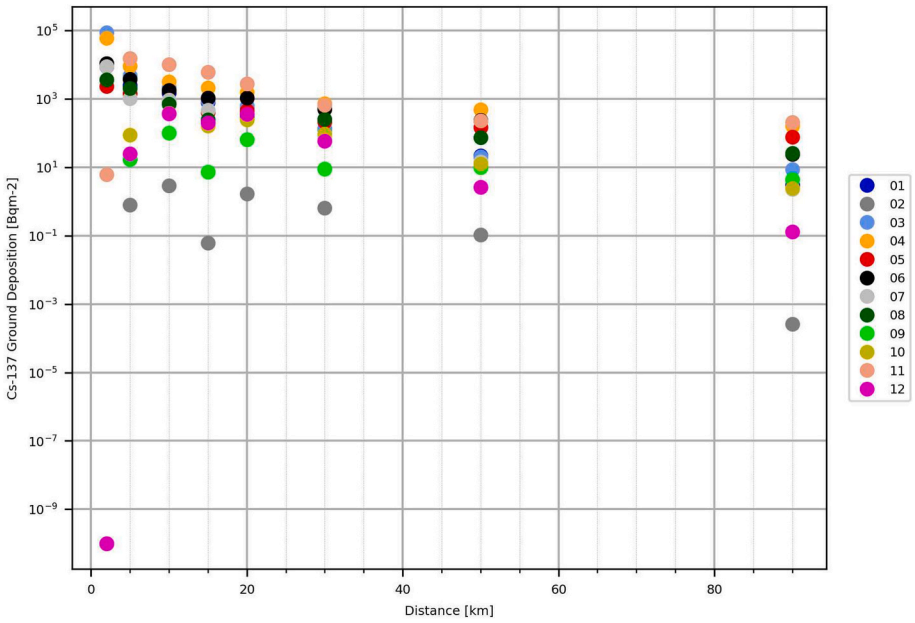

Fig. 10. WG-UA-1 – Cs-137 ground deposition at 120 h at 30 degrees.

Due to the relatively limited number of participants in WG-UA-2, it was not possible to extract solid mean trends.

5.2. Comparison at selected locations

Some of the most relevant population centres close to the release point were taken for comparison, in particular, Nikopol, Kryvyi Rih, Zaporizhzhia, and Melitopol.

As for WG-UA-1, the agreement is very similar to the one characterizing the preceding section for locations at specific distances and cardinal directions from the release point.

As for WG-UA-2, there are again no clear trends, and the results differ even in several orders of magnitude. Figs. 15–18 provide examples for various FOMs for both WG-UA-1 and WG-UA-2.

5.3. Comparison of average quantities at sector level

The goal of extending the comparison to the sector level was to eliminate potential biases that could dominate the significant discrepancies found at specific locations.

As expected, the agreement at sector level is much higher than at pointwise location, with most results differing by about one order of magnitude. The averaging technique used in this comparison analysis is unique and has no equivalent at the full computational grid level. At the full grid level, comparisons typically involve selecting specific geographic locations, whereas here, an average of an entire geographical region serves as the figure of merit for comparability. Averaging at sector level smooths out potential extreme values, leading to better agreement among the results.

Figs. 19–22 provide examples of these results, showing the trends of

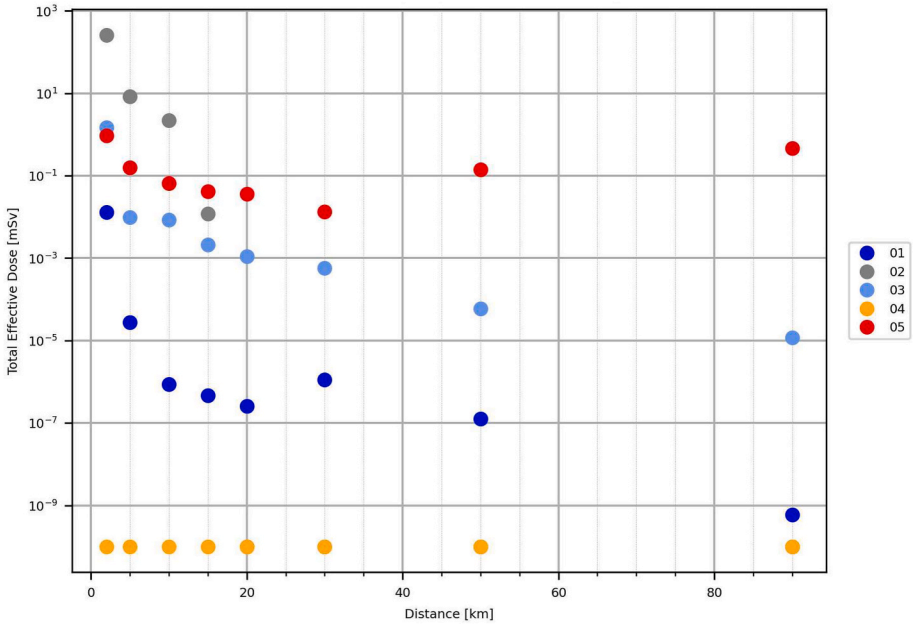

Fig. 11. WG-UA-2 TEDE at 36 h and 240 degrees.

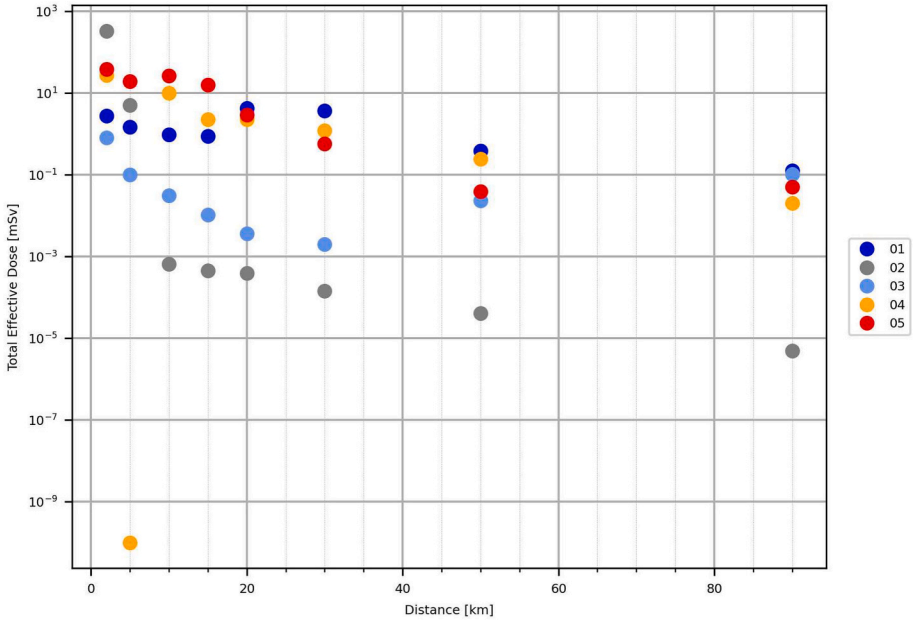

Fig. 12. WG-UA-2 – TEDE at 132 h at 300 degrees.

various figures of merit (FOMs), such as TEDE, Cs-137, and I-131 total ground deposition, averaged at sector levels for fixed hours after the emission started for the WG-UA-1 and WG-UA-2 exercises.

Further research into the potential benefits of using average values at the sector level to guide protective countermeasures is recommended.

5.4. Statistical analysis: Coefficient of variation

A statistical analysis of the outcomes was conducted using the Coefficient of Variation (CV) as an indicator.

For WG-UA-1, the main trend identified in the data comparison is that the CV for both the effective and equivalent thyroid doses ranges from 25 % to 150 %, with values reaching up to 300 % in regions far from the source. For WG-UA-2, the CV for all three figures of merit (FOMs) falls within 200 % for the region of interest, with values lower than those in WG-UA-1. Figs. 23–26 show the CV distribution maps for both WG-UA-1 and WG-UA-2.

Large CV values are primarily due to significant discrepancies between participants at certain locations along the computational grid, although most values are concentrated at the lower end.

5.5. Comparison of the maximum output values versus distance

The maximum output values have been compared at each geographical point from the source point along the whole computational grid. The main trends are the followings:

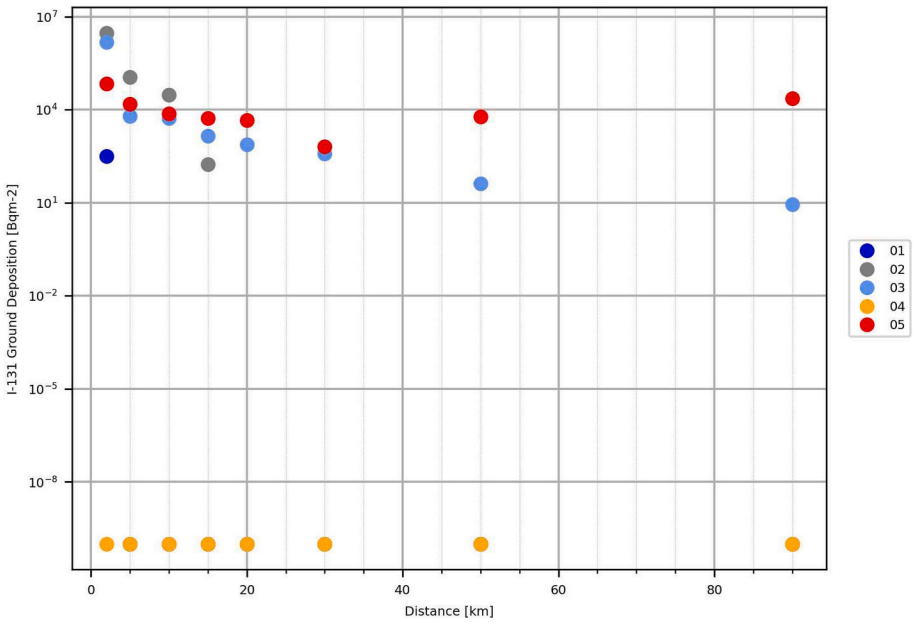

Fig. 13. WG-UA-2 – I-131 ground deposition at 36 h at 240 degrees.

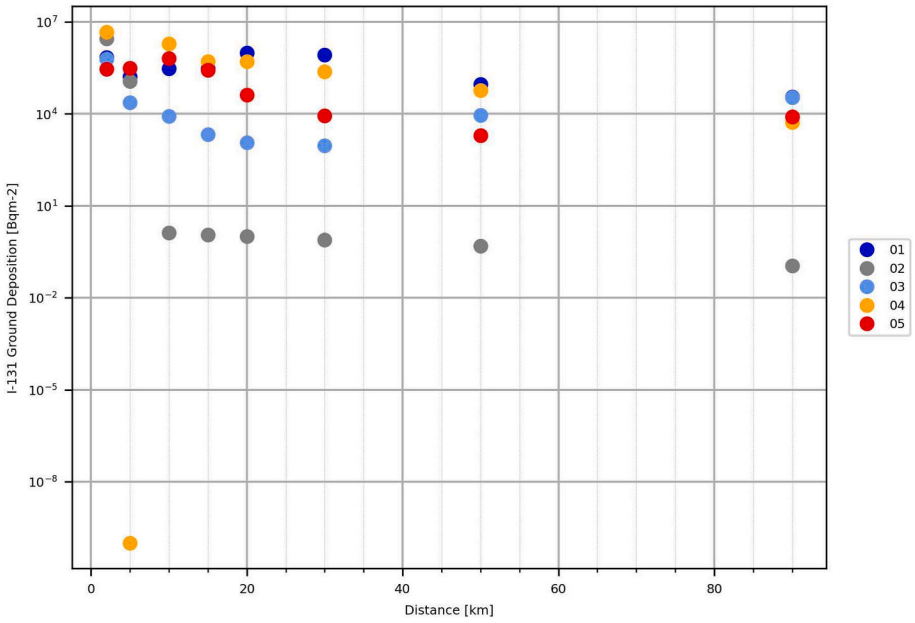

Fig. 14. WG-UA-2 – I-131 ground deposition at 132 h and 300 degrees.

- For WG-UA-1, the degree of divergence is significantly lower than one order of magnitude for nearly all participants, whereas for WG-UA-2 the discrepancy between the results is significant, encompassing several orders of magnitude.
- For WG-UA-1, the degree of divergence decreases with higher output values, consequently with longer elapsed times. It should be noted that the weather data used in the exercises may be reanalysed in most cases, rather than actual weather forecast data. Otherwise, the uncertainty on the weather prediction would have likely limited the level of convergence for increasing times.
- For WG-UA-1, given that all participants share the same source term, it is reasonable to assume that a dominant downwind path will concentrate most of the radioactive releases. Therefore, the maximum path output values exhibit a significant degree of convergence.
- For WG-UA-2, due to sharp differences in the source term used by each participant, the maximum output values along the maximum path trajectory show significant deviations. Similar trends for the differences among results apply to the three FOMs.
- For WG-UA-2, there is a higher convergence at lower distances from the source point, whereas the elapsed from the start of the releases seems not to play a role in the degree of discrepancy among the results.

Figs. 27-30 show the trend of FOMs versus distance following the maximum path value for all the participants of WG-UA-1 and WG-UA-2.

5.6. Comparison of the maximum output values at sector level

The maximum path at sector level was also analysed using the same

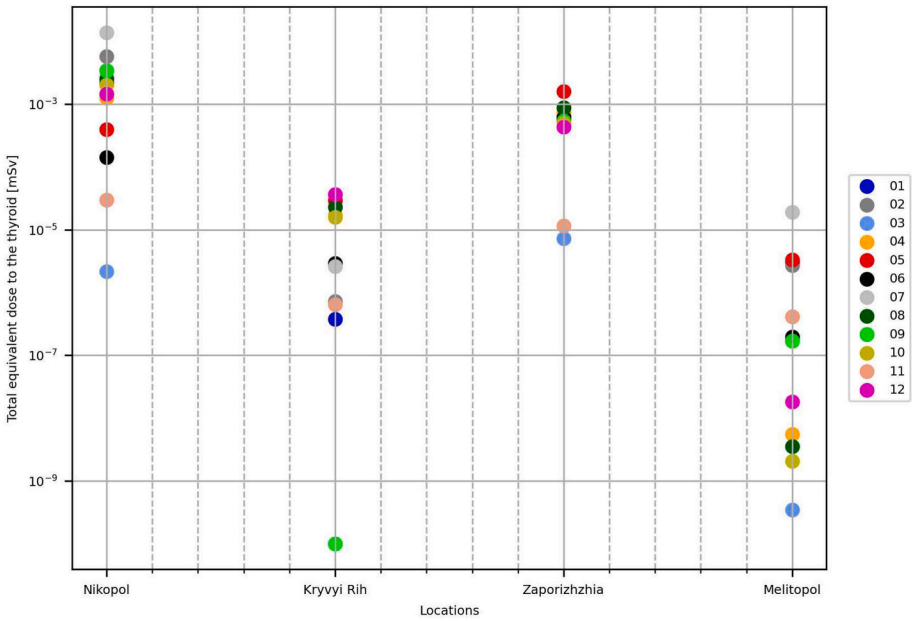

Fig. 15. WG-UA-1 – Thyroid equivalent dose at 240 h in selected locations.

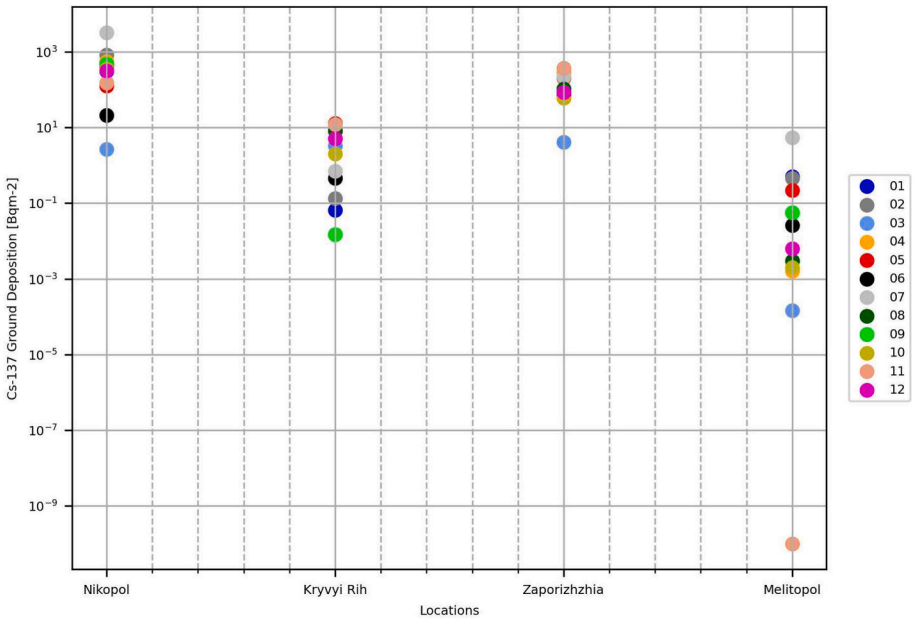

Fig. 16. WG-UA-1 – Cs-137 ground deposition at 240 h in selected locations.

methodology applied to the entire computational grid. Nonetheless, in this particular instance, both the region of points and the band within which the results fall is narrower. The sectors that accumulated the most radiological dispersion showed divergence levels well below one order of magnitude for almost all participants. This observation is consistent with the trends observed at full computational grid level. In general, it was observed that the degree of discrepancy is significantly higher (similar to the computational grid) in sectors that are less exposed, i.e., sectors that yield significantly lower results compared to those downwind, and in sectors at earlier times where the impact of a primary direction on radiological consequences is moderate.

The results for WG-UA-2 show similar trends to those observed at the point level. This sometimes allows for the identification of certain bands within which the results are contained, particularly at higher relative output values, although the dispersion can sometimes be very chaotic and wide.

Figs. 31 and 32 provide two instances of the maximum TEDE value at the sector level, along with the distance outcomes for all participants in the WG-UA-1 and WG-UA-2 exercises.

5.7. *Comparison of the maximum output values path on a map*

The geographical paths consisting of the set of geographical points featuring the maximum output values at each distance from the source point were developed for WG-UA-1 and WG-UA-2.

a) All participants predict a similar direction during the first 24 h, after which the discrepancies begin to expand geographically.
b) The degree of discrepancy in predicting the maximum path's geographical trajectory may be influenced by variations in weather

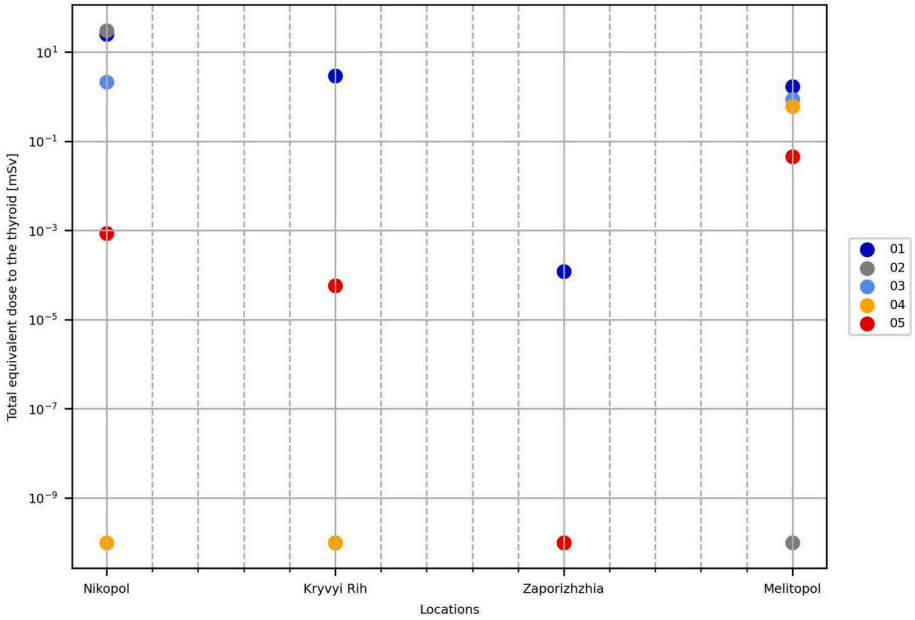

Fig. 17. WG-UA-2 – Thyroid equivalent dose at 96 h in selected locations.

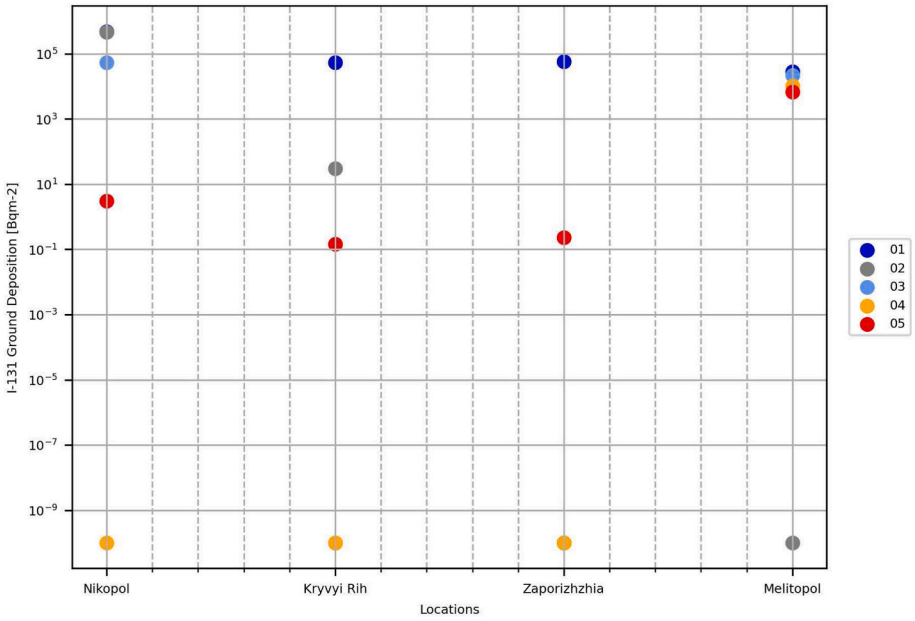

Fig. 18. WG-UA-2 – I-131 ground deposition at 180 h in selected locations.

forecast data and atmospheric dispersion modelling. However, since participants likely used reanalysed data, the significant discrepancies after the first 24–36 h from the start of releases are primarily related to the differences in atmospheric dispersion models and the use of different computational grid resolutions.

c) The different source terms used by the participants should not affect the maximum path's geographical trajectory, as the radiological consequences are linearly proportional to the magnitude of the source term.

Figs. 33-36 show the trend of the total effective equivalent dose maximum path on a geographic map for both WG-UA-1 and WG-UA-2.

5.8. *Country-to-Country comparison at different time instants*

A vis-à-vis comparison among participants taking all 2-combination sets for all the output variables and time instants at all geographical locations along the computational grid was performed for WG-UA-1 and WG-UA-2.

- For WG-UA-1, except for minimal and negligible values, there is a higher degree of convergence at higher output values, mostly due to the same underlying reason for a higher degree of convergence of the maximum path along the elapsed time from the start of the releases.
- For WG-UA-1, most of the points lie within plus minus two orders of magnitude.
- For WG-UA-2, there is a straightforward clear a trend towards a higher degree of convergence at lower times and average output

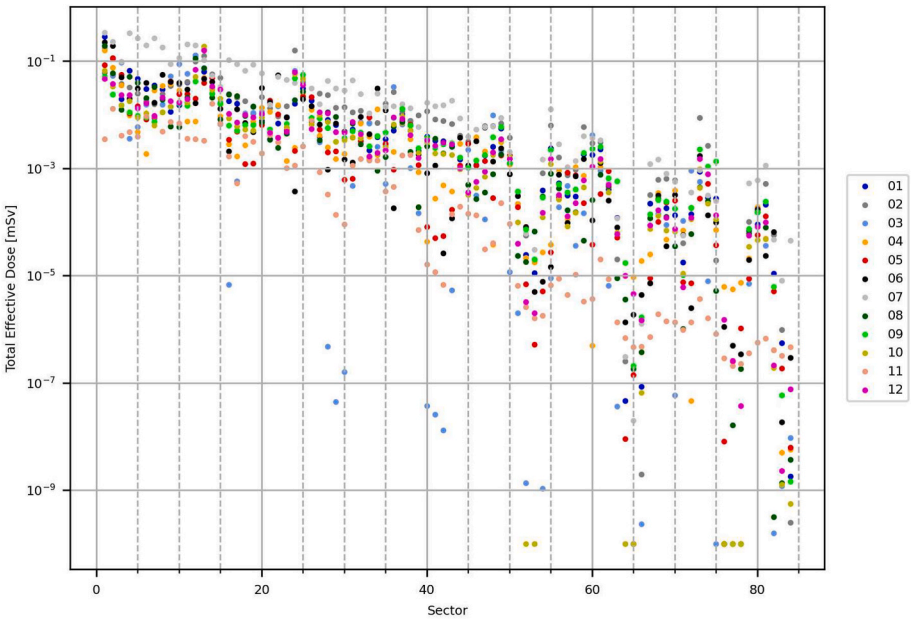

Fig. 19. WG-UA-1 – Total Effective Dose Equivalent at sector level average at 192 h.

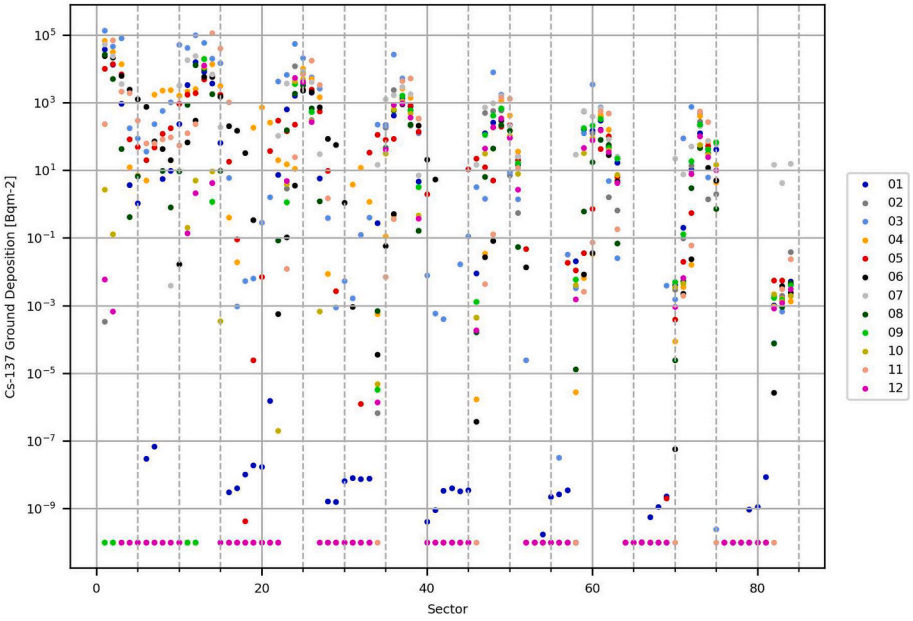

Fig. 20. WG-UA-1 – Cs-137 total ground deposition at sector level average at 168 h.

values for all three figures of merit. Such trend most probably has to deal with a more limited difference among the used source terms (whereas such difference increases with time). This trend is exactly opposite to the trend observed in WG-UA-1, where the differences in the weather forecast data were overcome by the relevance of the source term, similar for all the participants. It is to bear in mind that the high convergence degree at the beginning of the scenario is artificial, as it comes from the initial absence of radiological consequences (hence all values being zero).

- For WG-UA-2, Most of the points lie beyond two orders of magnitude once the difference among the predicted radioactive releases becomes bigger.

Figs. 37 and 38 show two examples of the country-to-country comparison trend for the TEDE at different time from the emission for both WG-UA-1 and WG-UA-2.

5.9. Country-to-Country comparison: trend analysis of the degree of convergence of the vis-à-vis comparison with the magnitude of output value

The relationship between the degree of convergence with the average output value was analysed. A similar trend to the previous comparison technique is observed, confirming the inversely proportional relationship between the degree of convergence and the elapsed time and average output value.

Figs. 39 and 40 report the trend of the TEDE convergence of the absolute value of the whole data in vis-à-vis time comparisons as the percentage of the convergence within one and two orders of magnitude.

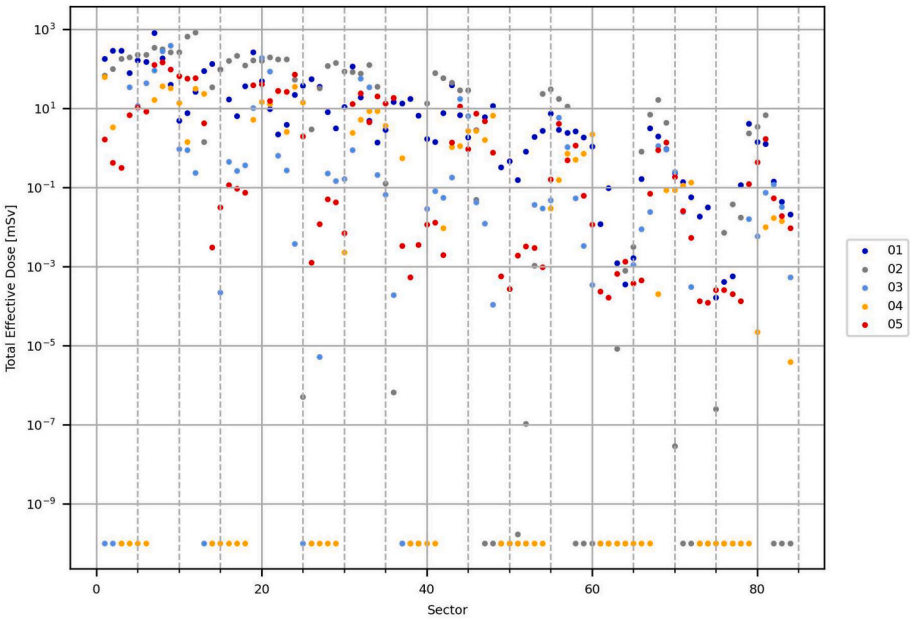

Fig. 21. WG-UA-2 – Total Effective Dose Equivalent at sector level average at 168 h.

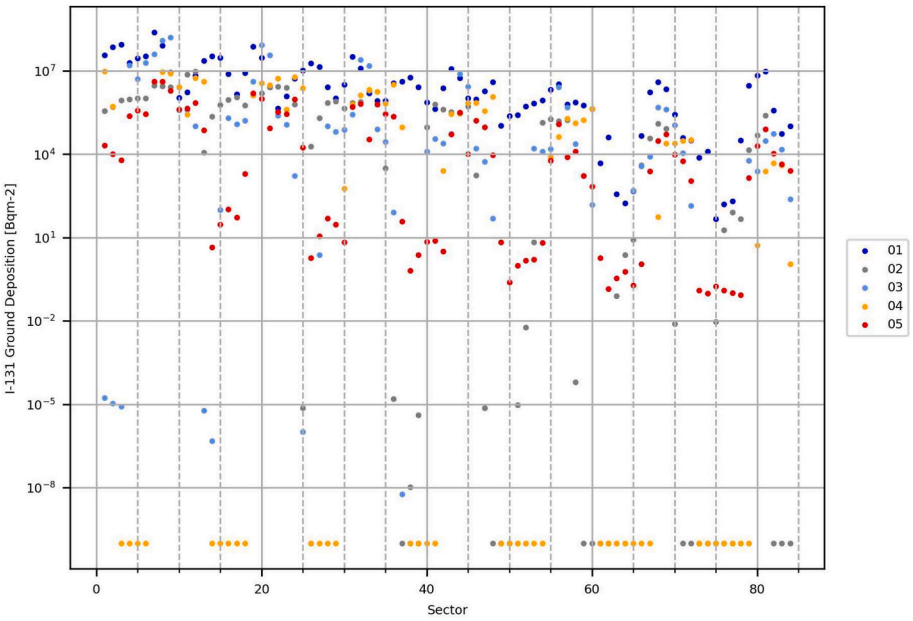

Fig. 22. WG-UA-2 – I-131 total ground deposition sector level average at 168 h.

5.10. *Country-to-Country comparison of the whole data*

The vis-à-vis comparison for the whole data together with the percentage of the total *integral mass value* within two orders of magnitude was analysed. The integral mass value is defined as the sum of the output values, each of which taken as a vis-à-vis arithmetic mean of the computed output value by each participant.

- Numerous points exhibit a significant degree of divergence.
- For WG-UA-1, there exists a distinct tendency towards a significantly higher degree of convergence at higher output values, which is applicable to the three figures of merits (although slightly less so for the deposited Cs-137)
- For WG-UA-1, there is a distinct tendency towards a higher degree of convergence at higher output values for all the three FOMs, except for minimal, negligible values. This is mostly due to the same underlying reason for a higher degree of convergence of the maximum.
- For WG-UA-2, there is no clear trend towards higher degrees of convergence at higher output values.
- This analysis enables to confirm that most values fall within a range of two orders of magnitude, particularly when values are not regarded as the number of points, but rather their value (i.e., mass)

Figs. 41 and 42 report the comparison for the whole data in a vis-à-vis absolute average comparisons for the three FOMs.

5.11. *Country-to-Country comparison of the whole data at sector level*

For both WG-UA-1 and WG-UA-2, the vis-à-vis comparison of the whole data together with the percentage of the total integral mass value

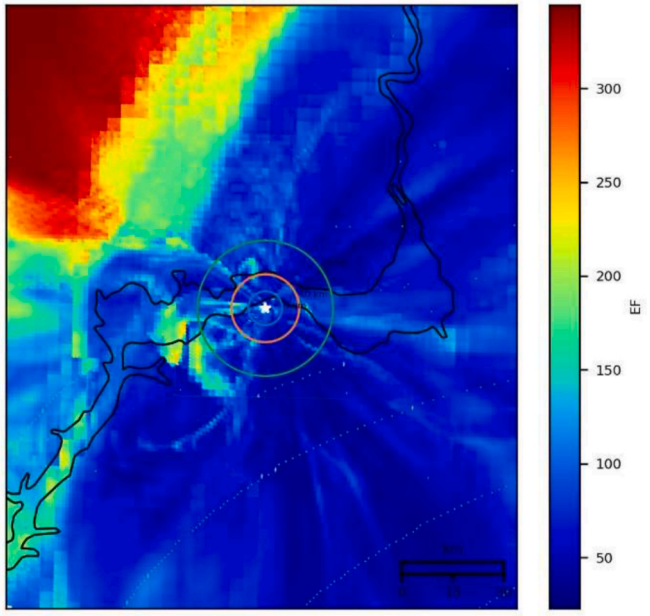

Fig. 23. WG-UA-1 – TEDE Coefficient of Variation (%) at 500 h.

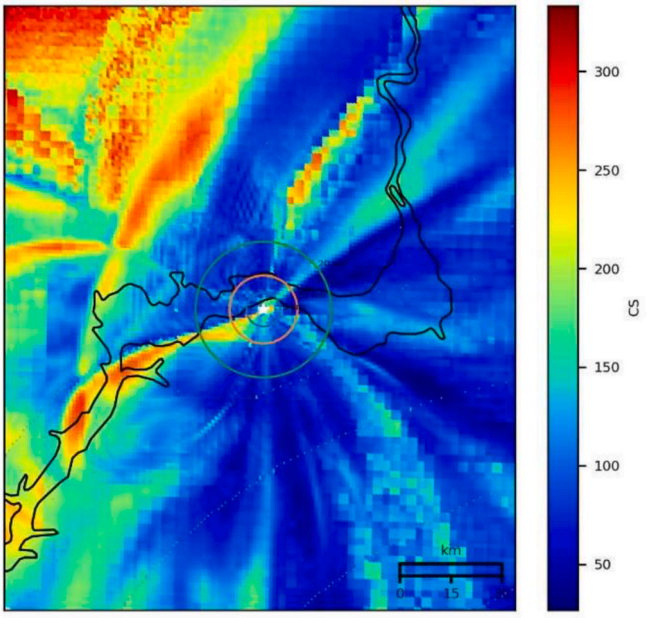

Fig. 24. WG-UA-1 Cs-137 ground deposition Coefficient of Variation (%) at 480 h.

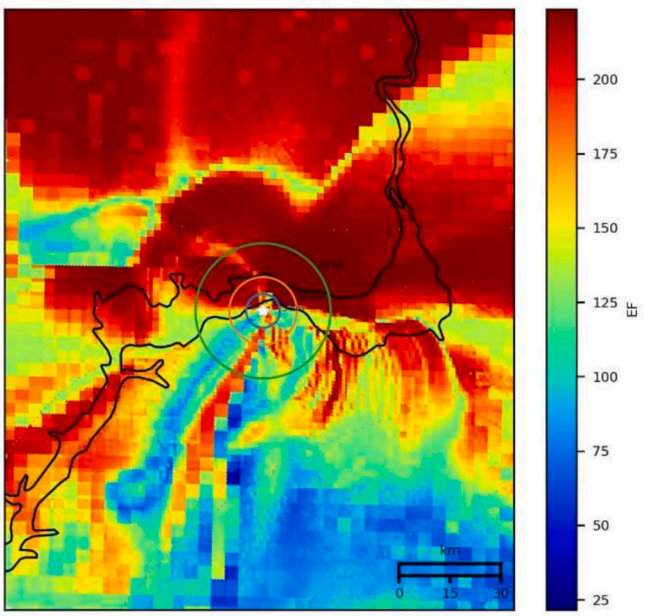

Fig. 25. WG-UA-2 – TEDE Coefficient of Variation (%) at 168 h.

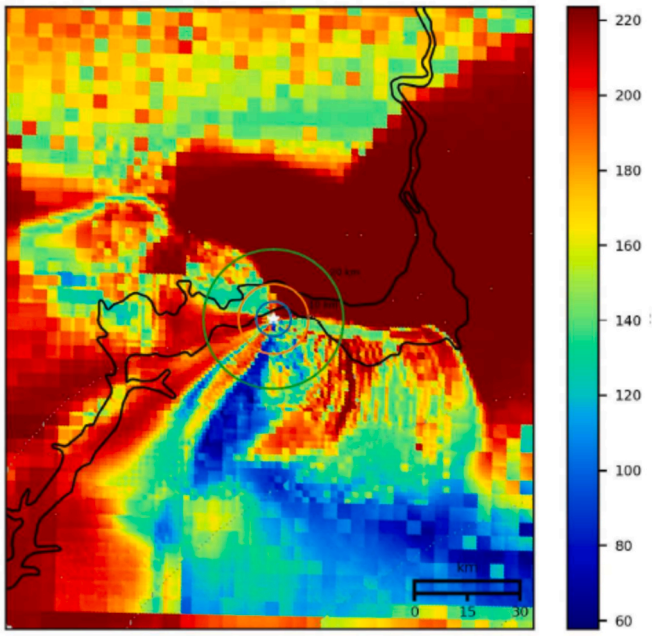

Fig. 26. WG-UA-2 – I-131 ground deposition Coefficient of Variation (%) at 168 h.

within two orders of magnitude was analysed at sector level.

For WG-UA-1, the degree of agreement between the output values is much better, given that the analysed area is lower. Specifically, almost all comparisons are kept within two orders of magnitude, though many of them falling entirely within one order of magnitude. At pointwise level, the dispersion between the results was lower with higher output relative values. This is confirmed at sector level where higher output concentrations have a higher degree of agreement, namely a higher percentage of values within one and two orders of magnitude.

For WG-UA-2, many points show an extremely high degree of divergence, but in this case, there is no clear trend towards higher degrees of convergence at higher output values.

Figs. 43 and 44 highlight the trend of the Total Effective Dose Equivalent convergence for the whole data at Sector 72 for WG-UA-1 and WG-UA-2 exercises.

6. Conclusion and recommendations drawn from the analysis of results

It should be noted that, as with any statistical analysis of a randomly distributed population, a thorough benchmarking exercise requires a large sample to draw sound conclusions on the underlying factors driving and/or characterizing the behaviour of the population. Since the analysis was limited to two exercises, WG-UA-1 and WG-UA-2, any conclusions drawn from them should be treated with caution.

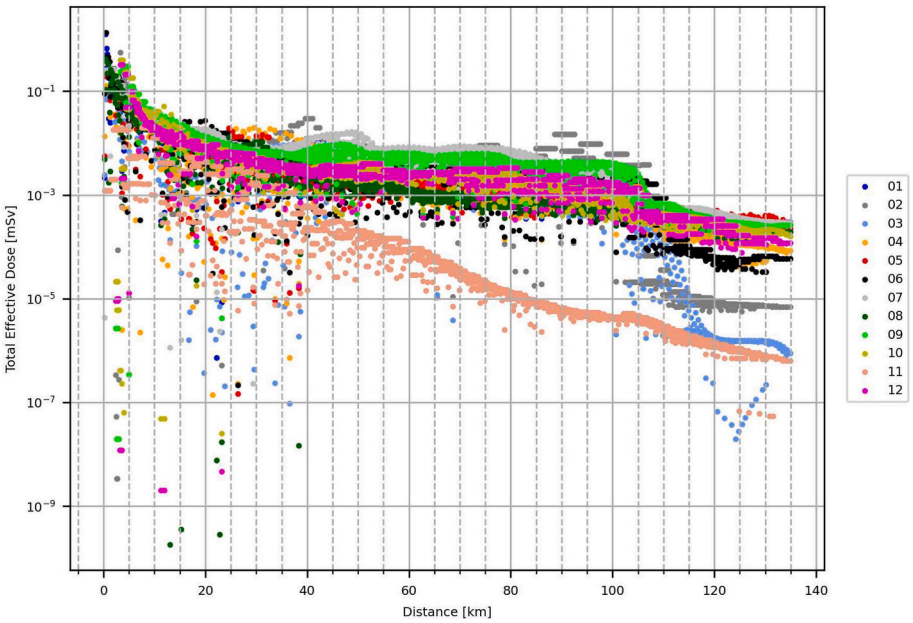

Fig. 27. WG-UA-1 – TEDE maximum path with distance at 168 h.

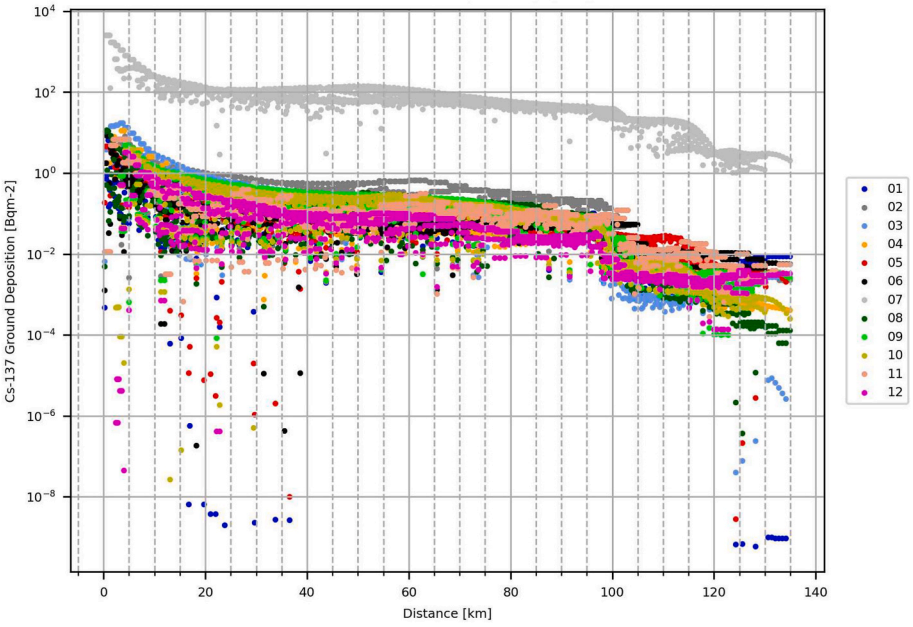

Fig. 28. WG-UA-1 – Cs-137 ground deposition maximum path with distance at 72 h.

Notwithstanding these limitations, trends have been identified, and underlying reasons have been provided. These reasons should be investigated through similar studies or follow-up exercises, such as an increase in the number of tests, sensitivity analysis, or theoretical analysis. The following general conclusions can be drawn from the analysis of the results:

- The source term magnitude has a strong impact on the discrepancy among the results as seen between WG-UA-1 and WG-UA-2.
- Despite the source term was fixed in WG-UA-1, the degree of discrepancy among the projected results does not significantly drop with distance or time but rather it remains unchanged for distances beyond dozens of kilometres and longer elapsed times from the start of the releases, most probably due to the higher sensitivity of the atmospheric diffusion at shorter distances from the source point.
- Most of the results fall within less than one order of magnitude up to two orders of magnitude for non-negligible output values in WG-UA-1, whereas for WG-UA-2 it is difficult to specify a range within which most of the values fall with high reliability.
- Although with the same source term (WG-UA-1), the discrepancies can still be significant for certain geographical locations, mainly due to the uncertainty coming from the atmospheric dispersion model and different weather forecast data (even if reanalysed).
- Narrower dispersion trends are observed at sector level due to limiting the comparison to smaller areas. In general, the comparison at sector level does not provide any novel particular insights to those

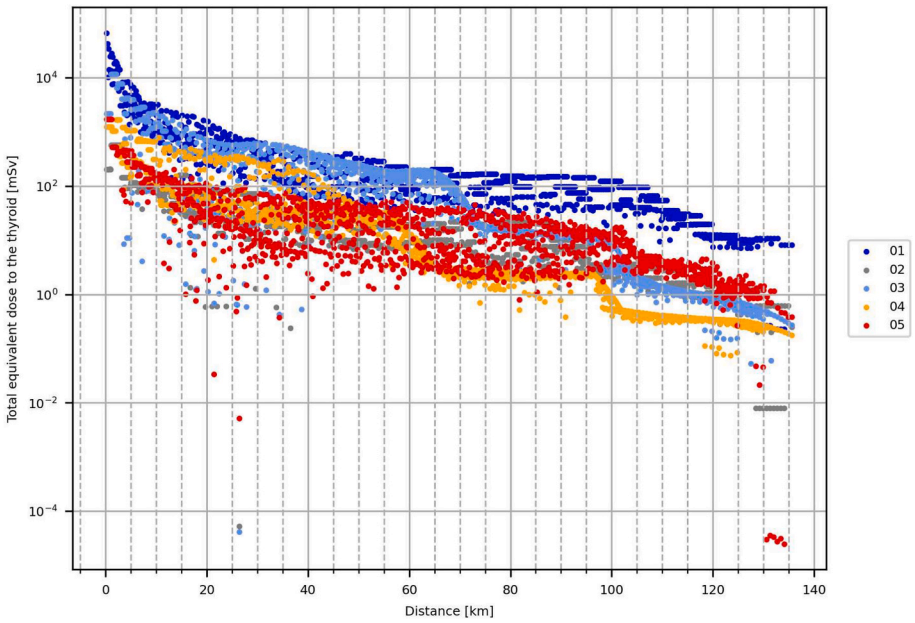

Fig. 29. WG-UA-2 – Thyroid equivalent dose maximum path with distance at 168 h.

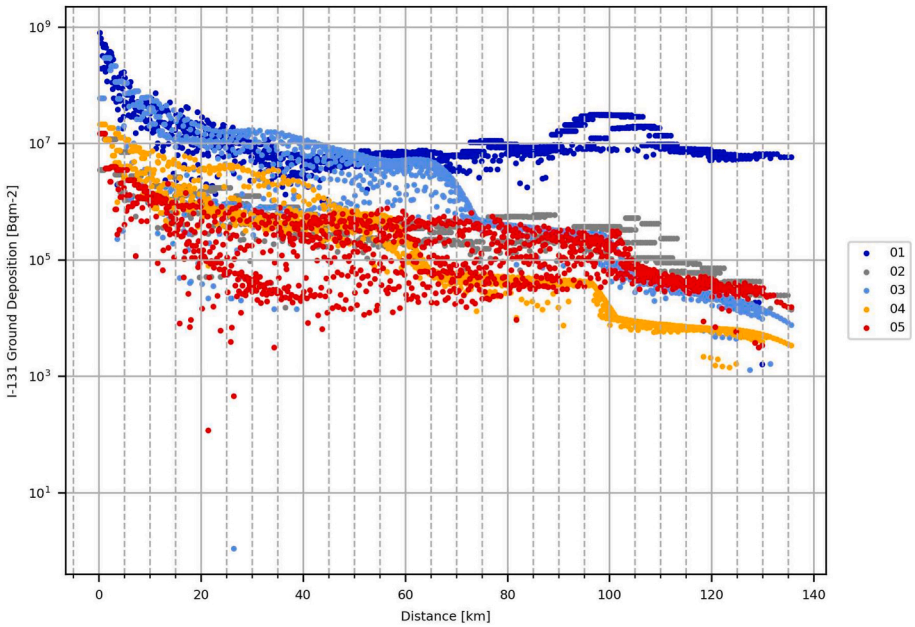

Fig. 30. WG-UA-2 – I-131 ground deposition maximum path with distance at 72 h.

previously identified at point level, taking the entire computational grid.

- As for WG-UA-1, the degree of discrepancy of the average values at sector level is inversely proportional to their relative magnitude, in other words, the higher the value (compared to the peak value), the lower the discrepancy, which seems to be related to the contribution of the source term to the results, whose weight overshadows the impact of the uncertainty of the weather forecast data and atmospheric dispersion model.
- The key sources of uncertainty are the source term, computational grid resolution, weather input data (both source and resolution) and atmospheric dispersion model.
- The impact of the cell size is twofold:
- Just like in any lumped-parameter model, coarse grids collapse the spatial distribution of results into a single point. Compared to models with finer computational resolution, this can lead to differences caused by the dilution of radionuclide concentration in the atmosphere.
- If the cell size is larger than the weather data resolution, such lumped effect will be even larger.
- The confidence of the weather data forecast is inversely proportional to the duration of the prognosis. However, it is noted that these benchmark exercises have considered reanalysed data, whose uncertainty is lower compared to actual weather forecast data.
- As for WG-UA-2, there are differences in the source term computed by each of the five participants, leading to major differences in the figure of merit. These differences are in the release magnitude, time and type of radionuclide, affecting both the cumulative dose and deposited material in magnitude and pace.

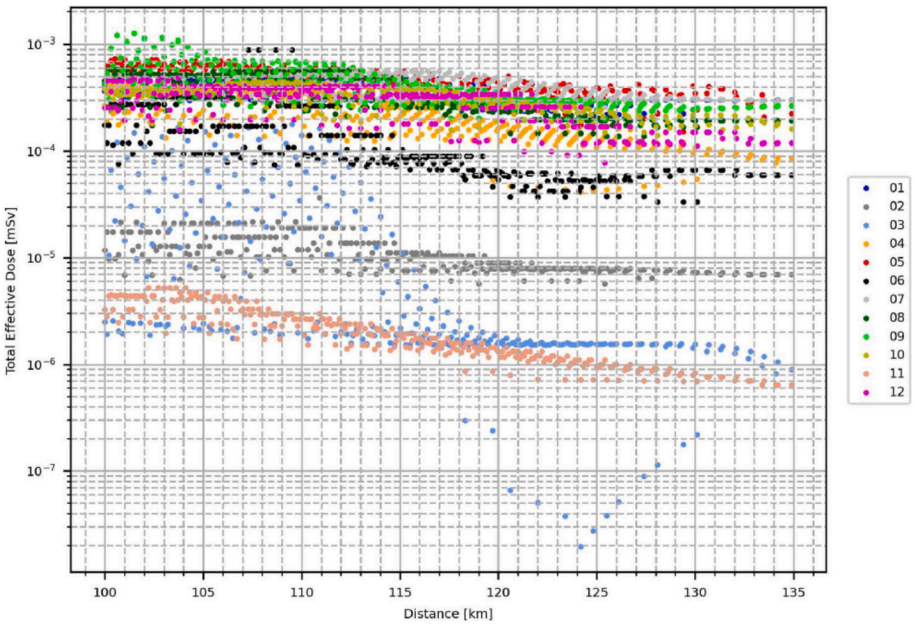

Fig. 31. WG-UA-1 – maximum TEDE for sector 74 at 168 h.

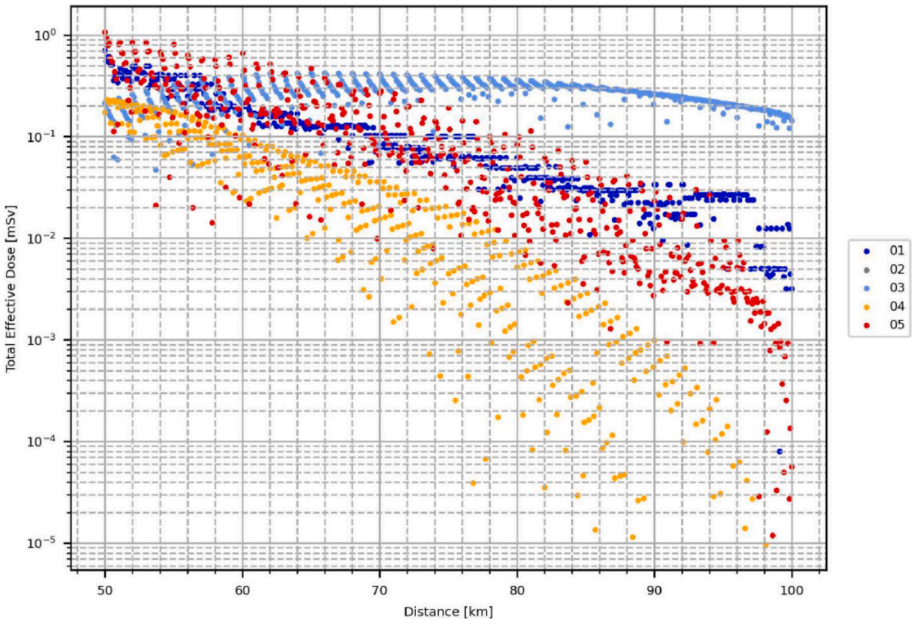

Fig. 32. WG-UA-2 – maximum TEDE for sector 70 at 96 h.

- The output values are cumulative values that can be schematically modelled as a function of an initial source strength –also called radioactive releases– subject to atmospheric dilution (advection and diffusion) along an exposure time.

$$FOM(r,t) = \int_0^{\Delta t_e} \overrightarrow{H}_w(\overrightarrow{r},t)\cdot S(t)\cdot dt$$

- The relative weight of each of these factors can be measured through an estimate of their respective order of magnitude:
- The dilution factor, $F_d(r,t)$, of the atmospheric stream on the transported radionuclides ranges between 1E and 09 and 1E-05 after 1–2 km from the source point.
- The source term, S(t), enough to require countermeasures, is a time-dependent function that can be as high as $1E+18$. The exposure time ranges around $1E+05$.
- The influence of the atmospheric stream on the radionuclide's mass is limited to the 0°-180° plane in the wind direction, which means that the radionuclide spreading upwind is negligible. This is considered through a dedicated factor, $\overrightarrow{H}_w$:

$$\overrightarrow{H}_w = \begin{cases} 1 \text{ if } \overrightarrow{r} > 0, & \textit{location is downwind} \\ 0 \text{ if } \overrightarrow{r} < 0, & \textit{location is upwind} \end{cases}$$

- Opposite forecast wind directions may lead to forceful discrepancies, as high as the source strength order of magnitude –especially for locations closer to 1 km from the source point.

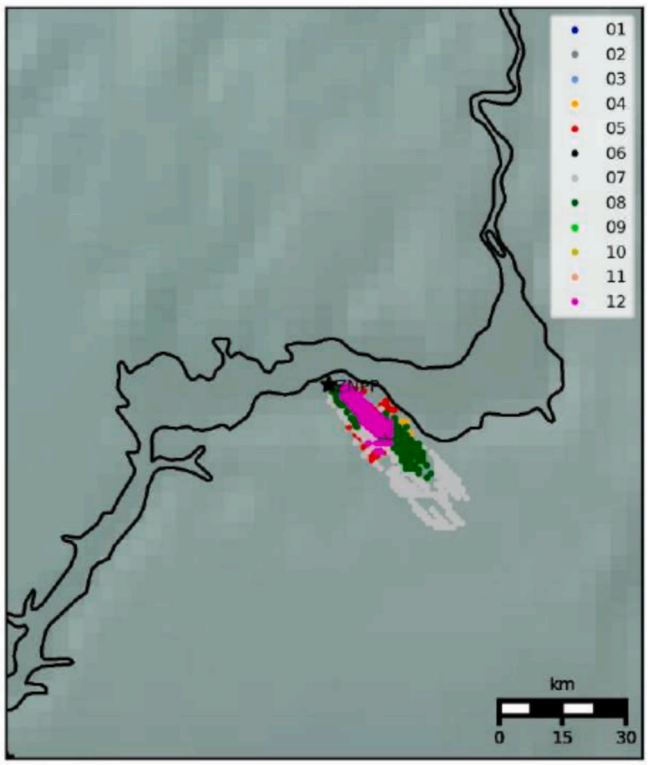

Fig. 33. WG-UA-1: TEDE maximum path on a geographic map at 24 h.

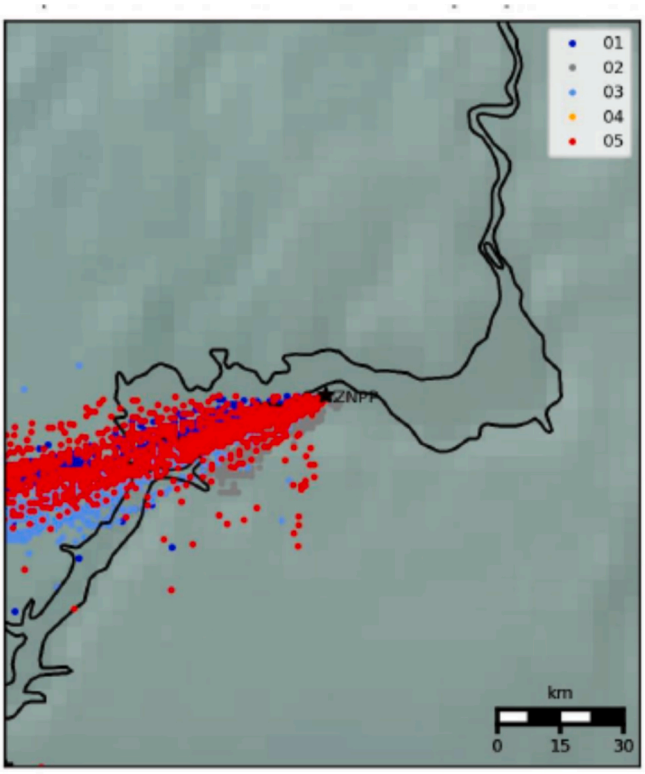

Fig. 35. WG-UA-2: TEDE maximum path on a geographic map at 24 h.

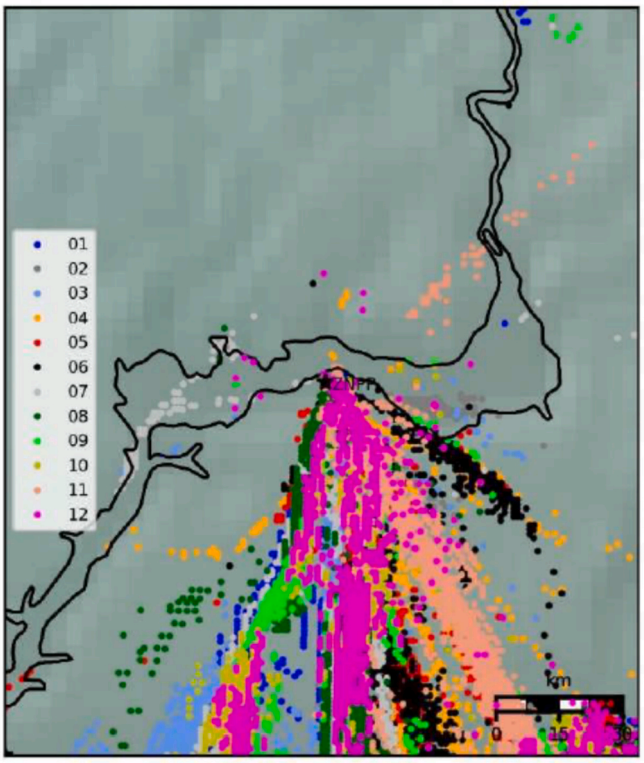

Fig. 34. WG-UA-1: TEDE maximum path on a geographic map at 480 h.

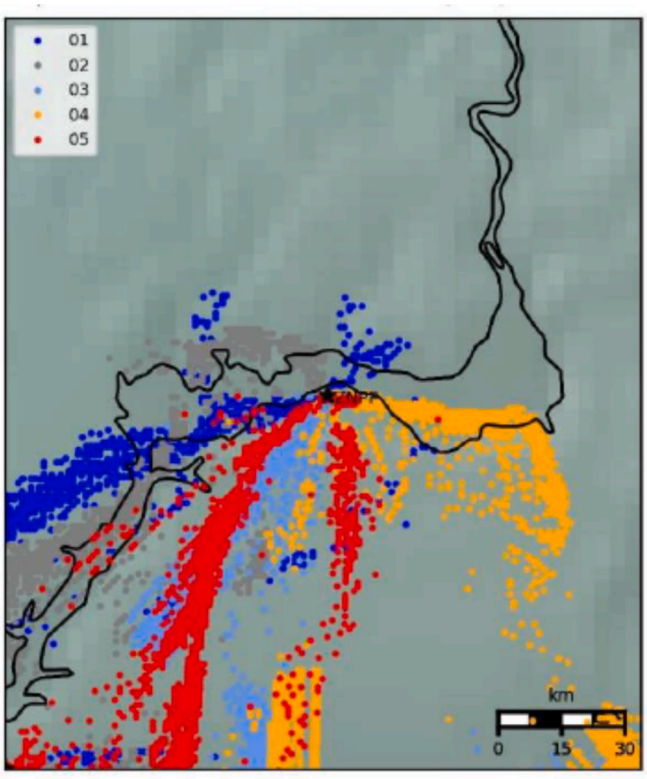

Fig. 36. WG-UA-2: TEDE maximum path on a geographic map at 120 h.

- From the schematic representation of the radiological consequences, it seems clear that the source term is the key factor behind the strong discrepancies found in WG-UA-2 compared to WG-UA-1, which does not mean that the dispersion model does not have a relevant contribution ranging around two orders of magnitude for similar wind directions, and as high as the source strength for different wind

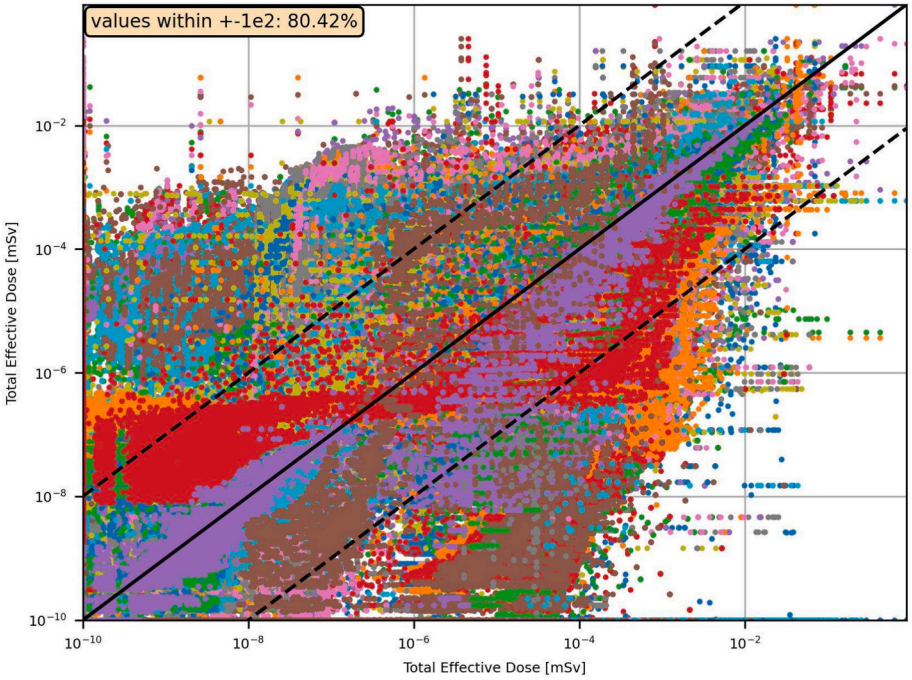

Fig. 37. WG-UA-1 TEDE Country-to-Country comparison at 120 h.

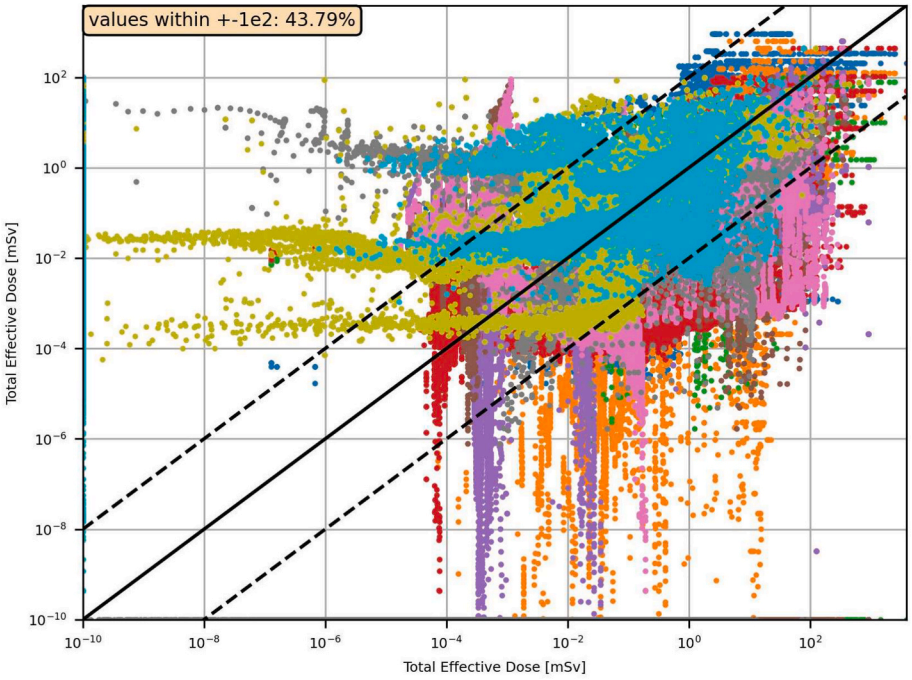

Fig. 38. WG-UA-2 TEDE Country-to-Country comparison at 168 h.

directions (the impact of the uncertainty of the weather forecast data is not fully considered in the current benchmarking exercises due to the fact of probably using reanalysed weather data by the participant organisations).

- Besides drawing general patterns of behaviour from the comparison of results, a detailed analysis based on focusing on specific discrepancies will also throw light on the understanding of the differences between the output values.

7. Recommendations on future activities

Discrepancies of the outputs related to cumulative dose and radionuclide contamination by using different modelling tools and source terms might be very high. Awareness of the reliability on the use of radiological consequence tools may be useful for the implementation of protective countermeasures.

Dose projection results should be used to the extent possible in combination with other alternative approaches, such as signals/observables of severe fuel damage, control room panel indicators, etc.

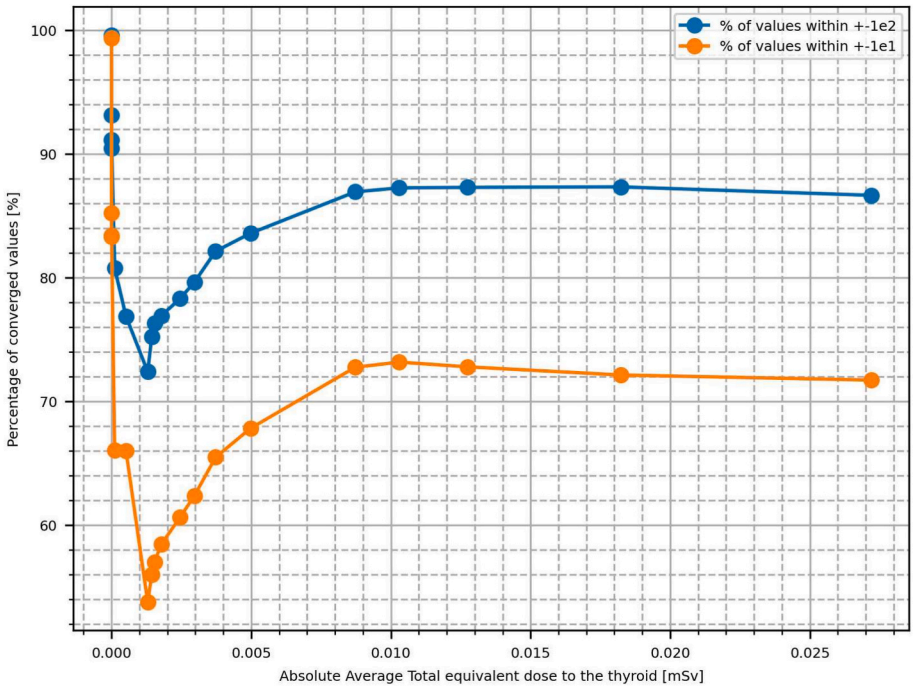

Fig. 39. WG-UA-1 Total equivalent dose to the thyroid – convergence of the whole data in a vis-à-vis ABS AVG comparison.

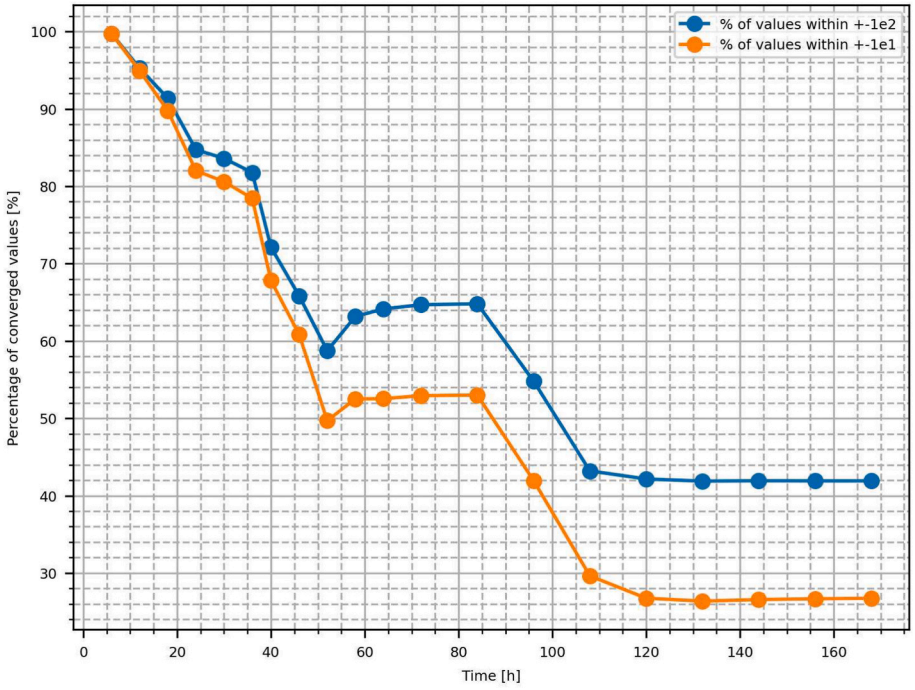

Fig. 40. WG-UA-2 Total equivalent dose to the thyroid – convergence of the whole data in a vis-à-vis ABS AVG comparison.

A reliable source term is essential to give credit to the results of any radiological consequence assessment. The calculation of the source term should account for the key driving aspects impacting the source term magnitude, speciation, and timing. The key phenomena on fission product releases, transport, and deposition (starting from precise initial conditions, namely the actual fission product inventory) and the behaviour of the last confinement barrier (within which severe accident phenomena impact to) should be carefully considered in the analytical tools used for computing a reliable source term. As for WG-UA-2, it appears that the tools used to calculate the source term have not met these criteria, which partly explains the much larger discrepancies compared to WG-UA-1.

The relation between the degree of discrepancy among the projected results (with fixed source term) with time and distance (both close and far-away) **should be further analysed** to identify latent cliff-edge effects on the uncertainty of radiological-consequence figures of merit, this way making an effective and reliable use of dose projection tools.

Even if the phenomena behind the radionuclides and last confinement behaviour are well represented, there are still **significant**

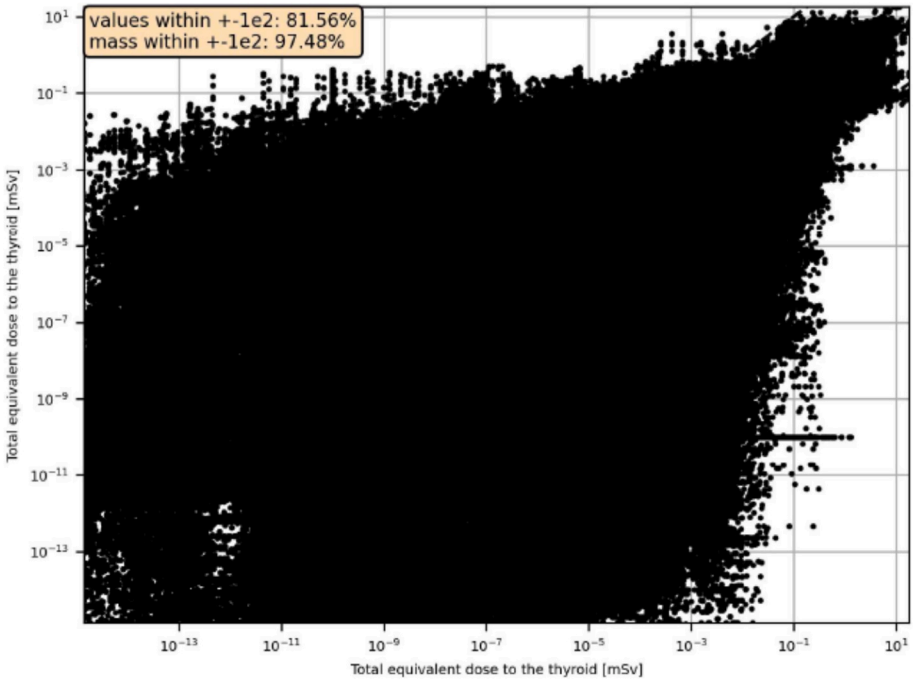

Fig. 41. WG-UA-1 Total equivalent dose to the thyroid – Convergence of the whole data.

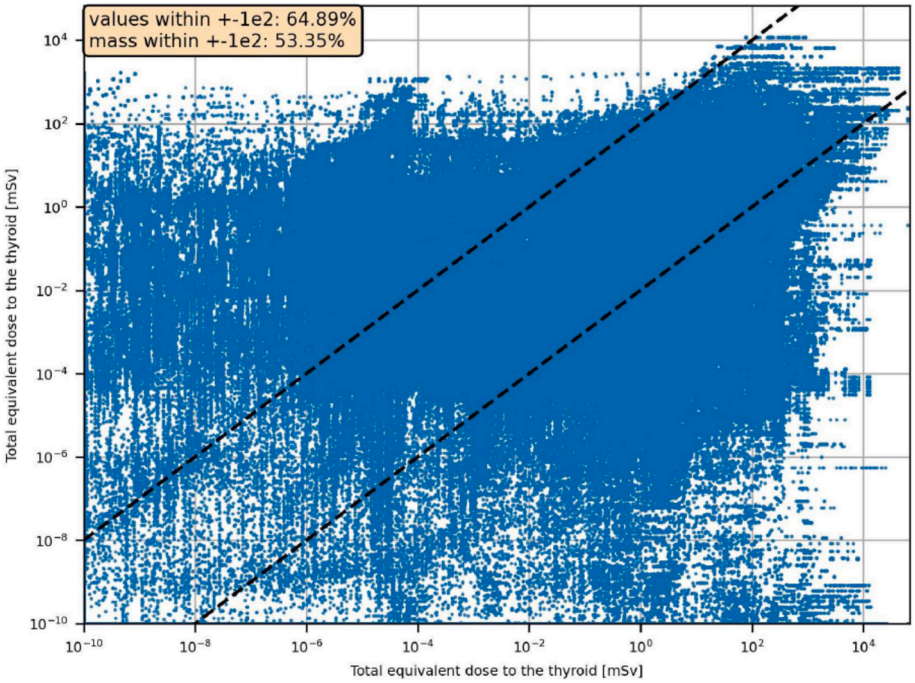

Fig. 42. WG-UA-2 Total equivalent dose to the thyroid – Convergence of the whole data.

uncertainties featured by current state-of-the-art severe accident analytical tools. Furthermore, severe accident scenarios leading to major releases to the outside environment would likely occur with additional uncertainties on some of the driving phenomena behind the behaviour of the last confinement barrier, such as Molten Core Corium Interaction or the loss of integrity of containment penetrations. To increase the robustness of the radiological consequence results, it is recommended to follow the past and ongoing research projects focused on the benchmarking of radiological consequence tools, and take their conclusions into account, with the aim of eventually integrating either correction factors for the propagation of uncertainty sources through the models, or through a posteriori uncertainty bands directly on the output values.

Harmonized guidelines on best practices and recommendations on the use of radiological consequence tools would substantially help dealing with the source term calculation, specific grid cell size, and computational grid, atmospheric model suitable with the scenario, weather data resolution, uncertainty implementation, and other relevant user effects.

Due to the chaotic nature of weather, namely slight variations in

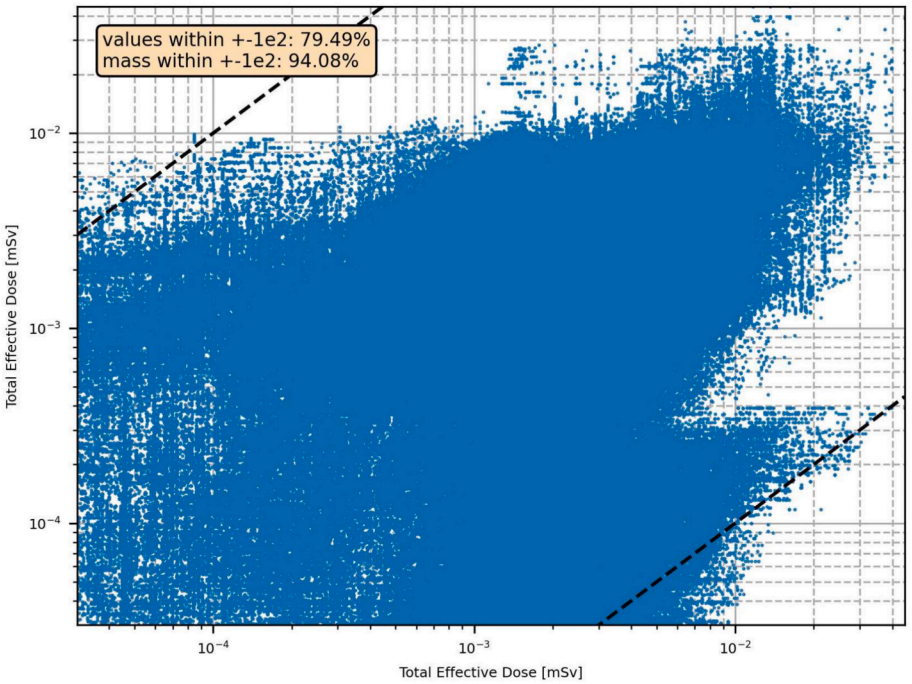

Fig. 43. WG-UA-1 TEDE – Sector 72 – Convergence of the whole data.

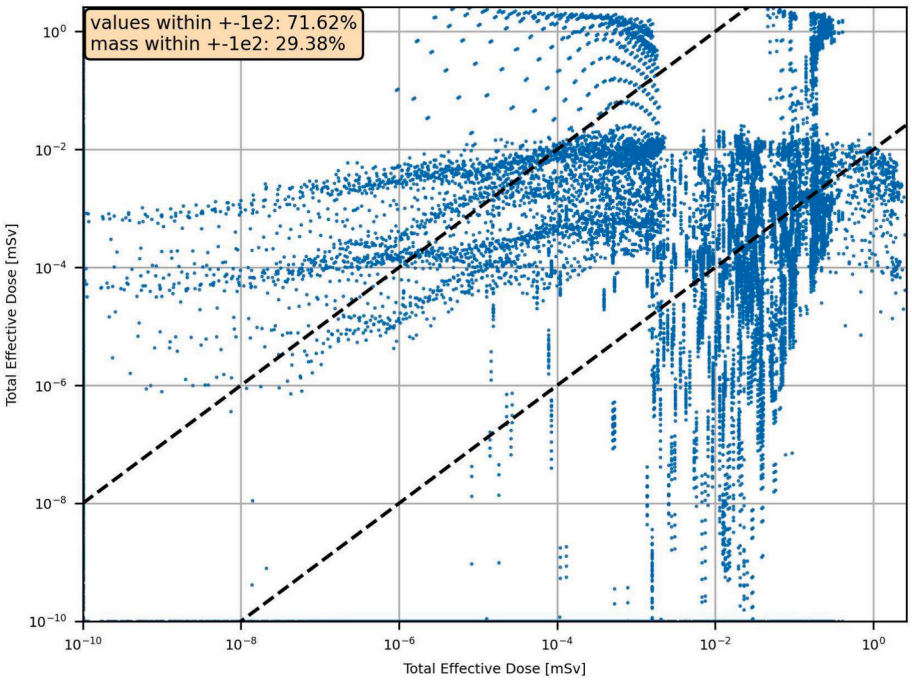

Fig. 44. WG-UA-2 TEDE – Sector 72 – Convergence of the whole data.

the inputs leading to very large variations in the outputs, it will not always be possible to reduce the uncertainty fully. A standard way to tackle this issue is by including the uncertainty bounds of the weather inputs rather than performing a single calculation. The systematic application of the well-defined clustering techniques could be a reliable strategy to evaluate the uncertainty in weather forecast data.

The **maximum path** –taken as maximum output values– as a high-confident indicator driving the implementation of protective countermeasures should be further analysed in view of the much lower degree of discrepancy found in WG-UA-1 for all the radiological-consequence figures of merit.

As it has been highlighted in the analysis of results, the degree of **discrepancy is lower at higher relative output values**. Given that protective countermeasures are driven by higher relative values, further comparison analysis exercises should only take the portion of the results featuring the maximum values, which can be easily highlighted **via the maximum path at area sector level**.

Based on the sustained (yet not entirely) higher degree of convergence among the output values for WG-UA-1 at sector level, **recommendations on deploying protective means should be based on**

maximum-path values at sector level rather than guided by single-point geographical coordinates. Follow-up comparisons with fixed source term at sector level should confirm this relevant point.

Further research on the potential benefit of using average values at sector levels to orient protective means rather than point-wise geographical values is highly recommended, given the highly dispersed calculations at geographical point level. Hided peak values levelled up through averaging can be accounted for by assigning a certain computational band to the results, which means that this inherent shortcoming of using average values can easily be compensated this way.

Given the existing significant discrepancies among the results, notably coming from the source term (though not only), it is key to ensure that the main information on the accident plant and scenario is available to develop and use an appropriate source term, which is also an important reason promoting in Europe the **early sharing of the information and the need of strengthening the coordination** among ECURIE Competent Authorities (especially since not all the organisations and countries have the same capabilities in the field).

Given the uncertainties associated with dose projection tools, **it becomes even more important to have in place a comprehensive radioactivity monitoring network**, even though such networks are not of any assistance for prompt decisions taken in the early phase of an accident, i.e. before the start of the release. Follow-up comparison and analysis of radiological consequence tools should be performed with the aim of confirming or rejecting the patterns identified in the current exercises. New analysis should use actual weather forecast data rather than reanalysed data to account for the actual uncertainty coming from this key source of information.

Funding information

The authors declare that no funding was received for the research or preparation of this manuscript.

CRediT authorship contribution statement

J.C. De la Rosa Blul: Conceptualization, Formal analysis, Investigation, Methodology, Software, Supervision, Writing – original draft, Writing – review & editing. **A. Guglielmelli:** Writing – review & editing, Supervision, Data curation. **O. Parera Villacampa:** Software, Investigation. **S. Arndt:** Software, Investigation. **S. Band:** Software, Investigation, Data curation. **S. Beck:** Software, Formal analysis, Data curation. **H. Boxman:** Software, Investigation, Data curation. **G. Fritsch:** Visualization, Software, Formal analysis, Conceptualization. **J. Groell:** Software, Formal analysis, Data curation. **T. Hamburger:** Supervision, Investigation, Data curation. **P. Hofer:** Software, Formal analysis, Data curation. **O. Isnard:** Validation, Supervision, Investigation, Formal analysis, Data curation. **A. Kloosterman:** Validation, Formal analysis, Data curation. **G.O. Nicaise:** Validation, Software, Formal analysis, Data curation. **A. Pašiškevičius:** Software, Data curation. **T. Peltonen:** Software, Data curation. **C. Potiriadis:** Validation, Software, Formal analysis, Data curation. **O. Romanenko:** Visualization, Supervision, Software, Investigation, Data curation. **N. Salpadimos:** Software, Formal analysis, Data curation. **A. Ševčik:** Software, Methodology, Formal analysis, Data curation. **M. Tempra:** Software, Investigation, Formal analysis, Data curation.

Declaration of competing interest

The authors declare that they have no known competing financial interests or personal relationships that could have appeared to influence the work reported in this paper.

Data availability

The data that has been used is confidential.

References

https://www.wenra.eu/rhwg. Access data: May 05, 2025.
https://www.herca.org/activity/emergency-preparedness-and-response/. Access date: May 05, 2025.
https://en.wikipedia.org/wiki/European_Community_Urgent_Radiological_Information_Exchange. Access date: May 05, 2025.
Balashevska, Y., Kyrylenko, Y., Ivanov, Z., Rocchi, F., Cervone, A., Guglielmelli, A., Ilvonen, M., Rossi, J., Slavickas, A., Thielen, H., 2024. Comparative analysis of the dispersion modelling and dose projection results performed under BARCO international project. J. Environ. Radioact. 279, 107513.
IAEA Coordinate Research Project, Effective use of dose projection tools in the preparedness and response to nuclear and radiological emergencies, 2019-22. https://www.iaea.org/projects/crp/j15002. Access date: May 05, 2025.
Nuclear Energy Agency, Expert Group on comparison and understanding of Dose Prognosis (EGDP), 2020-23. https://www.oecd-nea.org/jcms/pl_70963/expert-group-on-comparison-and-understanding-of-dose-prognosis-egdp. Access date: May 05, 2025.
https://www.wenra.eu/. Access date: May 05, 2025.
https://www.herca.org/. Access date: May 05, 2025.
Selivanova, A., Hůlka, J., Kotík, L., Kuča, P., Rubovič, P., Malátová, I., Helebrant, J., Koc, J., Rulík, P., Vlček, O., 2023. Advanced simulation techniques for the transport of routine atmospheric discharges using the JRODOS system. Prog. Nucl. Energy 157, 104596.
Murat, O., Sanchez-Espinoza, V., Gabrielli, F., Wang, S., Stieglitz, R., Queral, C., 2024. Improved analysis of the short-term station blackout accidents of the peach bottom unit-2 reactor with ASTEC including radiological impact and statistical analysis with JRODOS. Nucl. Eng. Des. 420, 113012.
Mercan, A.K., Gabrielli, F., Sanchez-Espinoza, V.H., Raskob, W., 2022. Analysis of the consequences of a LBLOCA with SBO severe accident in a generic VVER-1000 by means of ASTEC and JRODOS codes. Nucl. Eng. Design 400, 112078.
Dąbrowski, R., Kikoła, D., 2023. Application of atmospheric dispersion modelling in finding optimal locations of early warning stations around a nuclear power plant. Prog. Nucl. Energy 155, 104519.
Pirouzmand, A., Dehghani, P., Hadad, K., Nematollahi, M., 2015. Dose assessment of radionuclides dispersion from Bushehr nuclear power plant stack under normal operation and accident conditions. Int. J. Hydrogen Energy 40, 15198–15205.
Choi, G.-S., Lim, J.-M., Sunny Lim, K.-S., Kim, K.-H., Lee, J.-H., 2018. Characteristics of regional scale atmospheric dispersion around Ki-Jang research reactor using the Lagrangian Gaussian puff dispersion model. Nucl. Eng. Technol. 50 (1), 68–79.
Pirouzmand, A., Kowsar, Z., Dehghani, P., 2018. Atmospheric dispersion assessment of radioactive materials during severe accident conditions for Bushehr nuclear power plant using HYSPLIT code. Prog. Nucl. Energy 108, 169–178.
Orr, B., Hac-Heimburg, A., Syed, N.U.-H., Blixt Buhr, A.M., Ribeiro, L., Bergam, L., Ryan, R., Jaroszek, A., Ow, G., Dung, B.D., Pehrsson, J., 2023. Experiences from the ARGOS user group nuclear emergency exercise. J. Environ. Radioact. 270, 107298.
Orr, B., Hac-Heimburg, A., Syed, N.U.H., Buhr, A.M.B., Ribeiro, L., Bergman, L., Ryan, R., Jaroszek, A., Ow, G., Dung, B.D., Pehrsson, J., 2021. Intercomparison of transboundary atmospheric dispersion calculations: a summary of outputs from the ASEAN NPSR benchmark exercise. Prog. Nuclear Energy 135, 103718.
Dong, X., Zhuang, S., Fang, S., Li, H., Cao, J., 2021. Multi-scenario validation of CALMET-RIMPUFF for local-scale atmospheric dispersion modelling around a nuclear powerplant site with complex topography. J. Environ. Radioact. 229–230, 106547.
Quélo, D., Krysta, M., Bocquet, M., Isnard, O., Minier, Y., Sportisse, B., 2007. Validation of the polyphemus platform on the ETEX, chernobyl and Algeciras cases. Atmos. Environ. 41 (26), 5300–5315.
de la Rosa Blul, J.C., Parera Villacampa, O., Magrotti, G., Hernández Ceballos, M.Á., Pla Freixa, P., Ammirabile, L., Fazio, C., 2022. Application of the diagnosis and prognosis of hazards in nuclear emergencies (DAPHNE) tool to the Nuclear power plants in ukraine under war conditions. European Commission, Petten. JRC130447.
Jeong, H.S., Jeong, H.J., Kim, E.H., Han, M.H., Hwang, W.T., 2016. Assessment of fission product inventory considering axial burnup of a fuel assembly, Annals of Nuclear Energy, 2016, pp. 240-246.
Guglielmelli, A., Cervone, A., Rocchi, F., Creach, V., Ortega Nicaise, G., 2019. Intercomparison of PERSAN 4 and RASCAL 4.3 Source term evaluations for a PWR LOCA Scenario, Proceedings of EUROSAFE 2019, Köln.
Sato, I., Yoshikawa, S., Yamashita, T., Shimomura, K., Cibula, M., Mizokami, S., 2024. MAAP code analysis for the in-vessel phase of Fukushima-Daiichi Nuclear Power Station Unit 1 and comparison of the results among units 1 to 3. Nucl. Eng. Des. 422, 113088.
Sørensen, J.H., Bartnicki, J., Blixt, A.M., Lindgren, J., Schönfeldt, F., Sigg, R., 2020. Uncertainties in atmospheric dispersion modelling during nuclear accidents. J. Environ. Radioact. 222, 106356.